Baryon Asymmetry Transfer to Majorana Dark Matter from a Colored Partner*

Wei Huang (黄威) Hongjian Du (杜泓健) Feng Luo (罗峰) Michihisa Takeuchi

School of Physics and Astronomy, Sun Yat-sen University, Zhuhai 519082, China

Abstract: We propose a mechanism in which a primordial baryon asymmetry determines the relic abundance of self-conjugate dark matter through a heavier partner sector. In a simplified model with a Majorana fermion χ and a colored scalar partner $\tilde{q}$, QCD-mediated annihilations deplete the symmetric partner population, while a residual asymmetric component survives as a transient reservoir. For small portal couplings, this asymmetry is transferred to χ at late times, after dark matter freeze-out. The final relic abundance is controlled by the surviving asymmetry, the timing of its transfer, and subsequent dark matter annihilation.

By solving the coupled Boltzmann equations with the relevant chemical-potential effects, we find that an intermediate range of portal couplings can reproduce the observed relic abundance without requiring a compressed mass spectrum. This contrasts with conventional coannihilation and conversion-driven freeze-out scenarios, in which the heavier partner abundance is Boltzmann suppressed and a nearly degenerate spectrum, $m_{\tilde{q}} \simeq m_{\chi}$, is therefore typically required for the partner to remain sufficiently abundant to affect the dark matter relic abundance. In our mechanism, the relevant reservoir is the surviving asymmetric component of the partner population, which is not determined by the Boltzmann-suppressed thermal abundance of the heavier partner. Consequently, the mechanism can operate even for $m_{\tilde{q}} \gg m_{\chi}$.

The qualitative mechanism remains robust against variations in the mass hierarchy, dark matter annihilation mode, and lepton asymmetry. The small portal couplings also make the colored partner potentially long lived, allowing LHC searches for heavy long-lived particles to constrain part of the viable parameter space.

Keywords: Asymmetric dark matter, Baryon asymmetry transfer, Dark matterfreeze-out, Boltzmann equations, Long-lived particles

DOI: 10.1088/1674-1137/aeb48a **CSTR:**

CPC Accepted

I. INTRODUCTION

The coexistence of visible matter and dark matter (DM) in the Universe, together with their similar cosmological abundances, remains one of the central puzzles in modern cosmology. Astronomical observations indicate that the present-day dark matter density is approximately five times the baryonic matter density [1]. This numerical coincidence between the baryon and dark matter abundances has motivated the framework of asymmetric dark matter (ADM), in which the dark matter relic density is related to a primordial particle-antiparticle asymmetry [2−7]. A variety of mechanisms have been proposed to generate and transfer such an asymmetry between the visible and dark sectors [8−27].

In conventional ADM scenarios, the dark matter particle itself carries the conserved particle-antiparticle asymmetry that determines its relic abundance. However, this picture cannot be directly applied to a self-conjugate dark matter candidate, such as a Majorana fermion, for which the particle and antiparticle are identical. This raises a simple but important question: *can a primordial baryon asymmetry nevertheless determine the relic abundance of self-conjugate dark matter?*

In this work, we propose a mechanism that provides an affirmative answer to this question. The central idea is that the asymmetry need not be stored directly in the dark matter particle. Instead, a primordial baryon asymmetry can be shared between the Standard Model (SM) quark sector and a heavier partner sector, with the asymmetric component in the latter acting as a temporary reservoir. As the Universe evolves, this partner-sector asymmetry can survive the depletion of the symmetric component of

Received 25 August 2026; Accepted 14 October 2026

* M.T. is supported by the Fundamental Research Funds for the Central Universities, the One Hundred Talent Program of Sun Yat-sen University, China, and the Guangdong Natural Science Foundation (Project No. 2026A1515012641)

Content from this work may be used under the terms of the Creative Commons Attribution 3.0 licence. Any further distribution of this work must maintain attribution to the author(s) and the title of the work, journal citation and DOI. Article funded by SCOAP[3] and published under licence by Chinese Physical Society and the Institute of High Energy Physics of the Chinese Academy of Sciences and the Institute of Modern Physics of the Chinese Academy of Sciences and IOP Publishing Ltd

the partner population and subsequently be transferred to the SM quark sector through the decay of the partner into dark matter and a quark. At the same time, the amount of asymmetry that survives in the partner sector determines the abundance of the self-conjugate dark matter particle. This provides a qualitatively different realization of asymmetric dark matter, in which a self-conjugate dark matter particle can inherit its relic abundance from a primordial baryon asymmetry shared between the SM quark and partner sectors.

To realize this idea, we consider a simplified model containing a Majorana fermion χ, a complex scalar partner $\tilde{q}$, and an SM quark flavor q associated with the partner, with interactions described by

$$\mathcal{L}_{\text{portal}} = -\lambda \tilde{q}\bar{q}\frac{1-\gamma_5}{2}\chi + \text{h.c.}. \tag{1}$$

At sufficiently high temperatures, $T \gg m_{\tilde{q}}$, we assume that a net baryon asymmetry is distributed among the SM quark flavors and the $\tilde{q}$ sector. The origin of this distribution of the primordial asymmetry is not addressed in this work; it may arise from chemical equilibrium established through additional high-temperature interactions that become ineffective at lower temperatures, or from other dynamics in the dark sector. Instead, we focus on its subsequent cosmological evolution, in particular on how the asymmetry stored in the $\tilde{q}$ sector evolves and how its eventual transfer to the SM quark sector is correlated with the relic abundance of χ.

The essential dynamics are governed by the interplay between the rates of the $\tilde{q} \leftrightarrow \chi$ conversion processes and the Hubble expansion rate. For the epoch relevant to our mechanism, the total conversion rate is initially below the Hubble expansion rate, so the partner and dark matter sectors are not in chemical equilibrium. As the Universe cools, the conversion processes become effective at later times, during and after the thermal freeze-out of χ, while QCD annihilations deplete the symmetric component of the $\tilde{q}$ population. The asymmetric component is eventually transferred from $\tilde{q}$ to χ through decay or scattering processes, simultaneously contributing to the dark matter relic abundance and transferring the baryon asymmetry stored in the partner sector to the SM quark sector, as schematically illustrated in Fig. 1.

The magnitude of the asymmetric component that survives in the partner sector depends sensitively on the portal coupling λ. For sufficiently large λ, the late-time conversion is more efficient and the partner asymmetry is more strongly depleted, leaving only a small asymmetric component to be transferred to dark matter. In contrast, for sufficiently small λ, the surviving asymmetric excess can overproduce dark matter. The observed relic abundance is therefore obtained for an intermediate λ that allows a substantial but appropriately sized partner-sector asymmetry to survive.

For the benchmark mass choice $m_{\tilde{q}} = 2$ TeV and $m_\chi = 500$ GeV, we find that the observed dark matter relic abundance can be reproduced for a feeble coupling of order

$$\lambda \sim 10^{-9}. \tag{2}$$

The precise value depends on the mass spectrum and on the assumed primordial asymmetries. We quantify this cosmological evolution through a numerical solution of the coupled Boltzmann equations governing χ, $\tilde{q}$, and $\tilde{q}^*$.

An important feature of this mechanism is that it does not require the partner and dark matter states to be nearly degenerate. In conventional coannihilation scenarios [28], the abundance of the heavier partner is typically Boltzmann suppressed. Thus, a compressed spectrum, $m_{\tilde{q}} \simeq m_\chi$, is required for the partner to remain sufficiently abundant to influence the dark matter relic abundance. In the present framework, by contrast, the relevant quantity is the asymmetric component that survives the annihilation and conversion history, rather than the total thermal

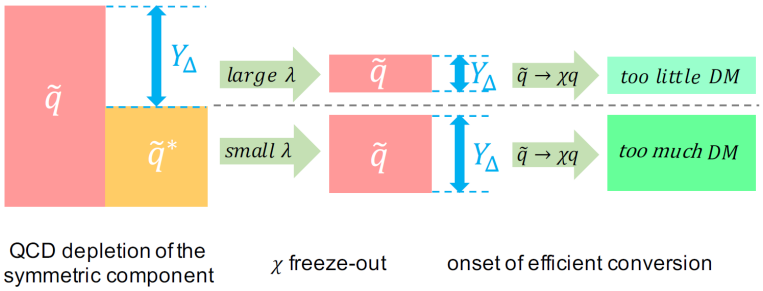

Fig. 1. (color online) Schematic illustration of the baryon asymmetry transfer mechanism. The sizes of the colored blocks indicate the relative number densities of the corresponding species. The primordial baryon asymmetry is distributed between the SM quark and partner sectors, with Y_Δ denoting the asymmetric component stored in the partner sector. The subsequent evolution involves QCD depletion of the symmetric partner component and late-time transfer of the surviving partner asymmetry to dark matter via $\tilde{q} \to \chi q$. The amount of asymmetry that survives in the partner reservoir depends on the portal coupling λ.

CPC Accepted

abundance of the partner. The partner can therefore act as an asymmetric reservoir even when it is significantly heavier than the dark matter, allowing the mechanism to operate for hierarchical spectra with $m_{\tilde{q}} \gg m_{\chi}$.

Our scenario also differs conceptually from conversion-driven freeze-out [29]. Although both frameworks involve feeble interactions between dark matter and a heavier partner, conversion-driven freeze-out is formulated for a symmetric dark sector, in which conversion processes control the freeze-out of the dark matter abundance. It likewise relies on a compressed mass spectrum, $m_{\tilde{q}} \simeq m_{\chi}$, so that the heavier partner remains sufficiently abundant during the non-relativistic evolution to maintain efficient conversion with dark matter. In our framework, by contrast, conversion processes control the survival and eventual transfer of a primordial asymmetry stored in the partner sector.

The feeble coupling required for efficient asymmetry transfer has an additional phenomenological consequence. Since $\tilde{q}$ is a colored scalar, its small coupling to χ and q can render it long-lived on detector timescales [30, 31]. After hadronization, such long-lived colored states form R-hadrons and can therefore be searched for through heavy stable charged particle (HSCP) signatures at the LHC [32, 33]. We use the ATLAS full Run-2 HSCP search results to constrain the parameter space for both $\tilde{t}$ and $\tilde{b}$ partner scenarios across their viable lifetime ranges. Thus, the same feeble coupling that enables the cosmological asymmetry-transfer mechanism also leads to potentially observable long-lived-particle signatures at colliders.

The remainder of this paper is organized as follows. In Sec. 2, we introduce the simplified model and derive the coupled Boltzmann equations governing the evolution of the relevant particle abundances and asymmetries. In Sec. 3, we discuss the treatment of chemical potentials and their role in closing the Boltzmann equations. In Sec. 4, we present the numerical results and investigate the dependence of the relic abundance on the model parameters. In Sec. 5, we study the collider constraints from long-lived-particle searches at the LHC. Finally, we summarize our main conclusions in Sec. 6.

II. THE MODEL AND BOLTZMANN EQUATIONS

A. Simplified model

To quantify the late-time dynamical evolution of the asymmetry transfer, we further specify the simplified model introduced in Sec. 1. In addition to the portal interaction $\mathcal{L}_{\rm portal}$ given in Eq. (1), the complex scalar partner $\tilde{q}$ is a color-triplet state that couples directly to the SM gauge fields through the gauge-kinetic term

$$\mathcal{L}_{\rm gauge} = (D_\mu \tilde{q})^\dagger (D^\mu \tilde{q}) . \tag{3}$$

Specifically, the covariant derivative acting on the color-triplet scalar $\tilde{q}$ is given explicitly by

$$D_\mu \tilde{q}_i = \left(\partial_\mu \delta_{ij} + i g_s T^a_{ij} A^a_\mu\right) \tilde{q}_j , \tag{4}$$

where g_s denotes the strong coupling constant, A^a_μ ($a = 1, \ldots, 8$) denotes the gluon gauge fields, and T^a are the $SU(3)_c$ generators in the fundamental representation, satisfying $\mathrm{Tr}(T^a T^b) = \frac{1}{2}\delta^{ab}$. These gauge interactions mediate rapid annihilation of $\tilde{q}\tilde{q}^*$ pairs, dominated by QCD processes, including Sommerfeld enhancement and bound-state effects [34–42]. They therefore efficiently deplete the symmetric component of $\tilde{q}$ in the early Universe while leaving a potentially nonzero asymmetric component.

Together with $\mathcal{L}_{\rm portal}$, these interactions define the simplified-model setup studied in Ref. [29] (see also Ref. [31] for a recent review), in which $\tilde{q}$ captures the essential gauge and portal dynamics of a right-handed squark in the Minimal Supersymmetric Standard Model (MSSM), without incorporating the full set of supersymmetric interactions. In particular, χ is not identified with a bino or another SM gaugino, and the portal coupling λ is treated as a free parameter within the simplified model.

Apart from $\mathcal{L}_{\rm portal}$, we do not explicitly specify the additional interactions responsible for maintaining the thermal history of χ. We assume that χ is initially in full chemical equilibrium with the thermal plasma and remains so until its ordinary thermal freeze-out. We take the corresponding number-changing interactions to be sufficiently efficient that

$$Y_\chi \simeq Y_\chi^{\rm eq} \tag{5}$$

at temperatures above the freeze-out temperature. After freeze-out, these interactions become inefficient, and Y_χ departs from its equilibrium value, leaving a residual thermal relic abundance.

For the parameter choices considered below, this standard thermal relic abundance is assumed to be subdominant to the observed dark matter abundance. The remaining dark matter abundance is subsequently generated by transferring the asymmetry stored in $\tilde{q}$ to the χ population. Thus, the mechanism studied here does not replace the standard thermal freeze-out of χ, but instead supplements its residual thermal relic abundance with an additional contribution sourced by the asymmetry in the partner sector.

For a Majorana fermion χ, such a thermal history can be realized through additional annihilation channels that

Chin. Phys. C Accepted

are not explicitly specified in the simplified model. For example, efficient p-wave annihilation through a CP-even Higgs-like scalar funnel can maintain chemical equilibrium at high temperatures and subsequently lead to standard thermal freeze-out. Alternatively, additional dark-sector states may participate in the annihilation processes, as in coannihilation scenarios analogous to slepton-neutralino coannihilation in the MSSM [43, 44]. The detailed ultraviolet realization of these additional interactions does not affect the asymmetry-transfer dynamics considered here; therefore, we parameterize their net effect through an effective $\chi\chi$ annihilation cross section.

The portal coupling λ is assumed to be sufficiently small that the interactions mediated solely by the portal do not maintain chemical equilibrium between χ and $\tilde{q}$ during the relevant late-time evolution. In particular, the conversion processes induced by λ can become inefficient relative to the Hubble expansion rate well before the QCD annihilations of the symmetric $\tilde{q}$ population cease. Consequently, the χ and $\tilde{q}$ abundances cannot be described by a common chemical-equilibrium condition, and their evolution must be followed separately.

B. Cross sections and rates

Using the Lagrangians in Eqs. (1) and (3), we employ the Mathematica package FeynCalc [45] to compute the tree-level spin- and color-averaged squared invariant amplitudes $|\overline{\mathcal{M}}|^2$ for the reactions appearing in the Boltzmann equations. The relevant processes and their dependence on the coupling parameters are summarized in Table 1. Collectively, these reactions determine the dynamical evolution of the $\tilde{q}$ asymmetry and its transfer to the χ sector.

We classify the reactions according to their roles in the asymmetry-transfer dynamics. Here, conversion processes are defined as reactions that directly exchange particle number between the $\tilde{q}$ and χ sectors. They include both the decay and inverse-decay process $\tilde{q} \leftrightarrow \chi q$ and the $2 \to 2$ conversion scatterings $\tilde{q}g \leftrightarrow q\chi$ and $\tilde{q}\bar{q} \leftrightarrow \chi g$. Although these two classes of conversion processes have different coupling dependences, both change the relative abundances of $\tilde{q}$ and χ. The decay and inverse-decay rates are proportional to λ^2, whereas the conversion scatterings involve one portal vertex and one QCD vertex and therefore scale as $\lambda^2 g_s^2$. In contrast, the process $\tilde{q}\chi \leftrightarrow qg$ is treated separately as a coannihilation process. Although this process also changes both Y_χ and $Y_{\tilde{q}}$, it removes a $\tilde{q}$ and a χ simultaneously rather than converting one species into the other. We therefore classify it as coannihilation rather than conversion.

In the parameter region relevant to the asymmetry-transfer mechanism, the portal coupling λ is much smaller than the strong coupling g_s, with g_s of order unity. Consequently, the portal-mediated processes are parametrically suppressed relative to the QCD interactions. In particular, the small portal coupling prevents $\tilde{q}$ and χ from remaining in chemical equilibrium as the Universe cools. Instead, the two sectors can depart from chemical equilibrium, allowing the pre-existing asymmetry stored in $\tilde{q}$ to be transferred to χ through out-of-equilibrium conversion processes.

The coupling dependences summarized in Table 1 allow us to simplify the coupled Boltzmann equations. The strong-interaction processes[1] $\tilde{q}\tilde{q}^* \leftrightarrow q\bar{q}$ and $\tilde{q}\bar{q}^* \leftrightarrow gg$ depend solely on g_s and therefore provide rapid pair-annihilation processes independent of λ. They efficiently deplete the symmetric component of $\tilde{q}$ while leaving its asymmetry unaffected.

By contrast, the portal annihilation processes proportional to λ^4, namely $\tilde{q}\tilde{q} \leftrightarrow qq$, $\tilde{q}\tilde{q}^* \leftrightarrow \chi\chi$, and the portal-induced contribution to $\chi\chi \leftrightarrow q\bar{q}$, are strongly suppressed relative to the g_s^4 and $\lambda^2 g_s^2$ processes for $\lambda \ll g_s$. We therefore neglect these portal-induced processes in the coupled Boltzmann equations governing the $\tilde{q}$–χ asymmetry-transfer dynamics. This approximation does not imply that $\chi\chi$ annihilation is neglected altogether. As discussed in Sec. 2.1, the ordinary thermal freeze-out of χ is assumed to be controlled by additional interactions beyond the simplified model. Their net effect is parameterized by an effective annihilation cross section $\langle\sigma v\rangle_{\chi\chi}$, which determines the residual thermal relic abundance of χ, whereas the portal-mediated processes considered here govern the subsequent transfer of the $\tilde{q}$ asymmetry.

In addition to the processes listed in Table 1, electroweak processes are allowed by Eq. (3) and by the SM interaction Lagrangian, such as $\tilde{q}\tilde{q}^* \leftrightarrow ZH$ and $\tilde{q}\gamma \leftrightarrow q\chi$. These electroweak channels have been shown to be subdominant compared with the strong-interaction processes [29]. Moreover, as demonstrated in Sec. 4, the relevant

Table 1. Reaction types and their dependence on couplings.

Reaction type	Reaction	Coupling dependence
Conversion	$\tilde{q} \leftrightarrow \chi q$	λ^2
	$\tilde{q}g \leftrightarrow q\chi$	$\lambda^2 g_s^2$
	$\tilde{q}\bar{q} \leftrightarrow \chi g$	
Coannihilation	$\tilde{q}\chi \leftrightarrow qg$	$\lambda^2 g_s^2$
	$\chi\chi \leftrightarrow q\bar{q}$	
Portal annihilation	$\tilde{q}\tilde{q} \leftrightarrow qq$	λ^4
	$\tilde{q}\tilde{q}^* \leftrightarrow \chi\chi$	
QCD annihilation	$\tilde{q}\tilde{q}^* \leftrightarrow q\bar{q}$	g_s^4
	$\tilde{q}\tilde{q}^* \leftrightarrow gg$	

1) For $\tilde{q}\tilde{q}^* \leftrightarrow q\bar{q}$, we note that, owing to the s-channel gluon-mediated diagram, the final-state quark and antiquark need not have the flavor associated with $\tilde{q}$. In addition, although a t-channel χ-exchange diagram exists for this process, its contribution to $|\overline{\mathcal{M}}|^2$ is suppressed and negligible.

CPC Accepted

asymmetry-transfer dynamics are predominantly controlled by λ, with the λ^2 and $\lambda^2 g_s^2$ processes governing the relevant portal-induced rates. Including the electroweak interactions would therefore introduce only a minor numerical correction to the extracted value of λ, and we do not include them in our Boltzmann system.

All cross sections, multiplied by the corresponding relative velocity of the incoming particles in each process, entering the Boltzmann equations are thermally averaged and denoted by the brackets $\langle\cdot\rangle$, using the standard formula [46]

$$\langle\sigma_{ij}v\rangle n_i^{\rm eq} n_j^{\rm eq} = T\frac{g_i g_j}{256\pi^5}\int \frac{p_{ij}p_{ab}}{\sqrt{s}}|\overline{\mathcal{M}}|^2 K_1\left(\frac{\sqrt{s}}{T}\right)\mathrm{d}s\,\mathrm{d}\cos\theta, \tag{6}$$

where K_1 denotes the modified Bessel function of the second kind of order one. Here, g_i (g_j) represents the internal degrees of freedom of species i (j), whereas p_{ij} (p_{ab}) denotes the magnitude of the three-momentum of the initial-state (final-state) particles in the center-of-mass frame.

The thermally averaged decay rate $\langle\Gamma\rangle_{\tilde{q}\to\chi q}$ is related to the decay width $\Gamma_{\tilde{q}\to\chi q}$, evaluated in the rest frame of $\tilde{q}$, by

$$\langle\Gamma\rangle_{\tilde{q}\to\chi q} = \Gamma_{\tilde{q}\to\chi q}\frac{K_1(m_{\tilde{q}}/T)}{K_2(m_{\tilde{q}}/T)}, \tag{7}$$

where K_2 denotes the modified Bessel function of the second kind of order two.

C. Boltzmann equations

In standard coannihilation scenarios with sufficiently rapid inter-species conversion, chemical equilibrium among dark-sector particles is maintained until decoupling, allowing the relic abundance to be described by a single Boltzmann equation for the total abundance [28]. In our framework, however, the portal coupling λ is sufficiently small that the conversion rates between $\tilde{q}$ and χ can fall below the Hubble expansion rate $H(T)$. As a result, $\tilde{q}$ and χ do not necessarily remain in chemical equilibrium throughout their subsequent evolution.

To track this departure from chemical equilibrium accurately, we solve the coupled Boltzmann equations for Y_χ, $Y_{\tilde{q}}$, and $Y_{\tilde{q}^*}$. This treatment consistently describes the ordinary thermal freeze-out of χ, the QCD depletion of the symmetric component of $\tilde{q}$, and the subsequent transfer of the $\tilde{q}$ asymmetry to χ within a single framework.

It is convenient to use the number densities of the dark matter particle χ, the complex scalar $\tilde{q}$, and its antiparticle $\tilde{q}^*$, normalized by the entropy density s:

$$Y_\chi \equiv \frac{n_\chi}{s}, \qquad Y_{\tilde{q}} \equiv \frac{n_{\tilde{q}}}{s}, \qquad Y_{\tilde{q}^*} \equiv \frac{n_{\tilde{q}^*}}{s}. \tag{8}$$

To focus directly on the physically relevant quantities—namely, the total partner abundance

$$Y_\Sigma \equiv Y_{\tilde{q}} + Y_{\tilde{q}^*} \tag{9}$$

and the net asymmetry

$$Y_\Delta \equiv Y_{\tilde{q}} - Y_{\tilde{q}^*}, \tag{10}$$

We transform the system of Boltzmann equations into the sum and difference variables. The resulting coupled system for Y_χ, Y_Σ, and Y_Δ is

$$\begin{aligned}\frac{\mathrm{d}Y_\chi}{\mathrm{d}x} =& -\frac{xs}{H(m_\chi)}\left(1+\frac{T}{3g_{*s}}\frac{\mathrm{d}g_{*s}}{\mathrm{d}T}\right)\\ &\times\Bigg\{\langle\sigma v\rangle_{\chi\chi}\left[Y_\chi^2-(Y_\chi^{\rm eq})^2\right]\\ &+\langle\sigma v\rangle_{\tilde{q}\chi\to qg}\left[Y_\Sigma Y_\chi - Y_\chi^{\rm eq}\left(Y_{\tilde{q},\rm w}^{\rm eq}+Y_{\tilde{q}^*,\rm w}^{\rm eq}\right)\right]\\ &-\frac{1}{s}\langle\Gamma\rangle_{\tilde{q}\to\chi}\left(\frac{Y_\Sigma+Y_\Delta}{2}-Y_\chi\frac{Y_{\tilde{q},\rm w}^{\rm eq}}{Y_\chi^{\rm eq}}\right)\\ &-\frac{1}{s}\langle\Gamma\rangle_{\tilde{q}^*\to\chi}\left(\frac{Y_\Sigma-Y_\Delta}{2}-Y_\chi\frac{Y_{\tilde{q}^*,\rm w}^{\rm eq}}{Y_\chi^{\rm eq}}\right)\Bigg\},\end{aligned} \tag{11}$$

$$\begin{aligned}\frac{\mathrm{d}Y_\Sigma}{\mathrm{d}x} =& -\frac{xs}{H(m_\chi)}\left(1+\frac{T}{3g_{*s}}\frac{\mathrm{d}g_{*s}}{\mathrm{d}T}\right)\\ &\times\Bigg\{\frac{1}{2}\langle\sigma v\rangle_{\tilde{q}\tilde{q}^*}\left[(Y_\Sigma+Y_\Delta)(Y_\Sigma-Y_\Delta)-4Y_{\tilde{q},\rm w/o}^{\rm eq}Y_{\tilde{q}^*,\rm w/o}^{\rm eq}\right]\\ &+\langle\sigma v\rangle_{\tilde{q}\chi\to qg}\left[Y_\chi Y_\Sigma - Y_\chi^{\rm eq}\left(Y_{\tilde{q},\rm w}^{\rm eq}+Y_{\tilde{q}^*,\rm w}^{\rm eq}\right)\right]\\ &+\frac{1}{s}\langle\Gamma\rangle_{\tilde{q}\to\chi}\left(\frac{Y_\Sigma+Y_\Delta}{2}-Y_\chi\frac{Y_{\tilde{q},\rm w}^{\rm eq}}{Y_\chi^{\rm eq}}\right)\\ &+\frac{1}{s}\langle\Gamma\rangle_{\tilde{q}^*\to\chi}\left(\frac{Y_\Sigma-Y_\Delta}{2}-Y_\chi\frac{Y_{\tilde{q}^*,\rm w}^{\rm eq}}{Y_\chi^{\rm eq}}\right)\Bigg\},\end{aligned} \tag{12}$$

$$\begin{aligned}\frac{\mathrm{d}Y_\Delta}{\mathrm{d}x} =& -\frac{xs}{H(m_\chi)}\left(1+\frac{T}{3g_{*s}}\frac{\mathrm{d}g_{*s}}{\mathrm{d}T}\right)\\ &\times\Bigg\{\langle\sigma v\rangle_{\tilde{q}\chi\to qg}\left[Y_\chi Y_\Delta - Y_\chi^{\rm eq}\left(Y_{\tilde{q},\rm w}^{\rm eq}-Y_{\tilde{q}^*,\rm w}^{\rm eq}\right)\right]\\ &+\frac{1}{s}\langle\Gamma\rangle_{\tilde{q}\to\chi}\left(\frac{Y_\Sigma+Y_\Delta}{2}-Y_\chi\frac{Y_{\tilde{q},\rm w}^{\rm eq}}{Y_\chi^{\rm eq}}\right)\\ &-\frac{1}{s}\langle\Gamma\rangle_{\tilde{q}^*\to\chi}\left(\frac{Y_\Sigma-Y_\Delta}{2}-Y_\chi\frac{Y_{\tilde{q}^*,\rm w}^{\rm eq}}{Y_\chi^{\rm eq}}\right)\Bigg\}.\end{aligned} \tag{13}$$

Here, $x \equiv m_\chi/T$ is used as the time-evolution variable.

CPC Accepted

The entropy density s and the rescaled Hubble parameter $H(m_\chi)$ are defined as

$$s = \frac{2\pi^2}{45} g_{*s} T^3 = \frac{2\pi^2}{45} g_{*s} \frac{m_\chi^3}{x^3},$$
$$H(m_\chi) \equiv H(T) x^2 = \sqrt{\frac{4\pi^3 g_*}{45}} \frac{m_\chi^2}{m_{\rm pl}}, \tag{14}$$

where $m_{\rm pl} \simeq 1.22 \times 10^{19}$ GeV is the Planck mass, and g_{*s} and g_* denote the effective relativistic degrees of freedom for entropy and energy density, respectively [47].

The physical meaning of the chemical-potential-dependent equilibrium abundances $Y^{\rm eq}_{\tilde{q},{\rm w}}$ and $Y^{\rm eq}_{\tilde{q}^*,{\rm w}}$, as well as the generalized rates $\langle\Gamma\rangle_{\tilde{q}\to\chi}$ and $\langle\Gamma\rangle_{\tilde{q}^*\to\chi}$ appearing in Eqs. (11)–(13), can be understood from the corresponding detailed-balance relations.

The subscript "w/o" denotes the thermal equilibrium state evaluated at zero chemical potential, $\mu = 0$. Under the Maxwell–Boltzmann (MB) approximation[1)] the equilibrium number densities of quarks and scalar partners at $\mu = 0$ are

$$n^{\rm eq}_{q,{\rm w/o}} = n^{\rm eq}_{\tilde{q},{\rm w/o}} = \frac{g_q}{2\pi^2} \int_{m_q}^{\infty} E \sqrt{E^2 - m_q^2} \exp\left(-\frac{E}{T}\right)$$
$$\mathrm{d}E = \frac{g_q}{2\pi^2} T m_q^2 K_2\left(\frac{m_q}{T}\right), \tag{15}$$

and

$$n^{\rm eq}_{\tilde{q},{\rm w/o}} = n^{\rm eq}_{\tilde{q}^*,{\rm w/o}} = \frac{g_{\tilde{q}}}{2\pi^2} \int_{m_{\tilde{q}}}^{\infty} E \sqrt{E^2 - m_{\tilde{q}}^2} \exp\left(-\frac{E}{T}\right)$$
$$\mathrm{d}E = \frac{g_{\tilde{q}}}{2\pi^2} T m_{\tilde{q}}^2 K_2\left(\frac{m_{\tilde{q}}}{T}\right), \tag{16}$$

where $g_q = 6$ and $g_{\tilde{q}} = 3$ are the internal degrees of freedom of q and $\tilde{q}$, respectively. This representation in terms of modified Bessel functions is valid for arbitrary m_i/T and smoothly interpolates between the relativistic and nonrelativistic regimes.

Assuming that all SM particles remain in local thermal equilibrium, the number densities of quarks and antiquarks in the presence of the quark chemical potential μ_q satisfy

$$n_q = n^{\rm eq}_{q,{\rm w/o}} e^{+\mu_q/T}, \qquad n_{\bar{q}} = n^{\rm eq}_{\bar{q},{\rm w/o}} e^{-\mu_q/T}. \tag{17}$$

Here, μ_q denotes the chemical potential of the quark flavor associated with $\tilde{q}$, as discussed in detail in Sec. 3.

Detailed balance allows the collision terms governing the conversion processes to be expressed in a common form. For the scattering process $\tilde{q}g \leftrightarrow q\chi$, we have

$$\langle\sigma v\rangle_{q\chi\to\tilde{q}g} n^{\rm eq}_\chi n^{\rm eq}_{q,{\rm w/o}} = \langle\sigma v\rangle_{\tilde{q}g\to q\chi} n^{\rm eq}_{\tilde{q},{\rm w/o}} n^{\rm eq}_g. \tag{18}$$

Defining

$$\langle\Gamma\rangle_{\tilde{q}g\to q\chi} \equiv \langle\sigma v\rangle_{\tilde{q}g\to q\chi} n^{\rm eq}_g, \tag{19}$$

the corresponding collision term becomes

$$\langle\sigma v\rangle_{\tilde{q}g\to q\chi} n_{\tilde{q}} n_g - \langle\sigma v\rangle_{q\chi\to\tilde{q}g} n_q n_\chi$$
$$= \langle\Gamma\rangle_{\tilde{q}g\to q\chi} \left(n_{\tilde{q}} - n_\chi \frac{n^{\rm eq}_{\tilde{q},{\rm w}}}{n^{\rm eq}_\chi}\right), \tag{20}$$

where we also use $n_g = n^{\rm eq}_g$. The effective equilibrium density $n^{\rm eq}_{\tilde{q},{\rm w}}$ is defined as

$$n^{\rm eq}_{\tilde{q},{\rm w}} \equiv n^{\rm eq}_{\tilde{q},{\rm w/o}} e^{+\mu_q/T}. \tag{21}$$

We emphasize that this quantity does not correspond to an independent chemical potential for $\tilde{q}$, nor does it imply chemical equilibrium between $\tilde{q}$ and χ. Rather, it is an effective equilibrium density induced by the chemical potential of the SM-quark bath and enters the detailed-balance relation for the portal conversion processes. In Sec. 3, μ_q/T will be expressed in terms of the net yield Y_Δ, thereby closing the Boltzmann system self-consistently.

Using the yield $Y = n/s$, we accordingly define

$$Y^{\rm eq}_{\tilde{q},{\rm w}} \equiv Y^{\rm eq}_{\tilde{q},{\rm w/o}} e^{+\mu_q/T}, \qquad Y^{\rm eq}_{\tilde{q},{\rm w/o}} \equiv \frac{n^{\rm eq}_{\tilde{q},{\rm w/o}}}{s}. \tag{22}$$

Similarly, for the decay and inverse-decay processes $\tilde{q} \leftrightarrow \chi q$, detailed balance gives

$$\langle\Gamma\rangle_{\tilde{q}\to\chi q} n^{\rm eq}_{\tilde{q},{\rm w/o}} = \langle\sigma v\rangle_{\chi q\to\tilde{q}} n^{\rm eq}_\chi n^{\rm eq}_{q,{\rm w/o}}. \tag{23}$$

Thus, the corresponding net interaction term can be written as

$$\langle\Gamma\rangle_{\tilde{q}\to\chi q} n_{\tilde{q}} - \langle\sigma v\rangle_{\chi q\to\tilde{q}} n_\chi n_q = \langle\Gamma\rangle_{\tilde{q}\to\chi q} \left(n_{\tilde{q}} - n_\chi \frac{n^{\rm eq}_{\tilde{q},{\rm w}}}{n^{\rm eq}_\chi}\right). \tag{24}$$

1) The MB approximation is adopted here to simplify the evaluation of collision integrals in the Boltzmann equations, consistent with the derivation of Eqs. (6) and (7). In the absence of Bose condensation or Fermi degeneracy, MB statistics provides a good approximation and is commonly used in the treatment of Boltzmann equations [48, 49]. It also allows the chemical-potential dependence, $e^{\pm\mu_q/T}$, to be factored exactly out of the phase-space integrals, leading to a simple detailed-balance relation.

CPC Accepted

For decays of $\tilde{q}$ into χ and additional SM particles[1)], the corresponding collision terms can be incorporated using the same detailed-balance form, provided that the relevant SM chemical potentials are included consistently. We therefore use the notation

$$\langle\Gamma\rangle_{\tilde{q}\to\chi\mathrm{SM}}\left(n_{\tilde{q}}-n_{\chi}\frac{n^{\mathrm{eq}}_{\tilde{q},\mathrm{w}}}{n^{\mathrm{eq}}_{\chi}}\right) \tag{25}$$

for the net decay and inverse-decay contribution.

For the scattering process $\tilde{q}\bar{q}\leftrightarrow g\chi$, detailed balance requires

$$\langle\sigma v\rangle_{\tilde{q}\bar{q}\to g\chi}n^{\mathrm{eq}}_{\tilde{q},\mathrm{w/o}}n^{\mathrm{eq}}_{\bar{q},\mathrm{w/o}}=\langle\sigma v\rangle_{g\chi\to\tilde{q}\bar{q}}n^{\mathrm{eq}}_{g}n^{\mathrm{eq}}_{\chi}. \tag{26}$$

Defining

$$\langle\Gamma\rangle_{\tilde{q}\bar{q}\to g\chi}\equiv\langle\sigma v\rangle_{\tilde{q}\bar{q}\to g\chi}n^{\mathrm{eq}}_{\tilde{q},\mathrm{w/o}}, \tag{27}$$

the collision term becomes

$$\begin{aligned}&\langle\sigma v\rangle_{\tilde{q}\bar{q}\to g\chi}n_{\tilde{q}}n_{\bar{q}}-\langle\sigma v\rangle_{g\chi\to\tilde{q}\bar{q}}n_{g}n_{\chi}\\&=\langle\Gamma\rangle_{\tilde{q}\bar{q}\to g\chi}e^{-\mu_q/T}\left(n_{\tilde{q}}-n_{\chi}\frac{n^{\mathrm{eq}}_{\tilde{q},\mathrm{w}}}{n^{\mathrm{eq}}_{\chi}}\right).\end{aligned} \tag{28}$$

For the coannihilation process $\tilde{q}\chi\leftrightarrow qg$, detailed balance yields

$$\langle\sigma v\rangle_{\tilde{q}\chi\to qg}n^{\mathrm{eq}}_{\tilde{q},\mathrm{w/o}}n^{\mathrm{eq}}_{\chi}=\langle\sigma v\rangle_{qg\to\tilde{q}\chi}n^{\mathrm{eq}}_{q,\mathrm{w/o}}n^{\mathrm{eq}}_{g}, \tag{29}$$

which leads to

$$\begin{aligned}&\langle\sigma v\rangle_{\tilde{q}\chi\to qg}n_{\tilde{q}}n_{\chi}-\langle\sigma v\rangle_{qg\to\tilde{q}\chi}n_{q}n_{g}\\&=\langle\sigma v\rangle_{\tilde{q}\chi\to qg}\left(n_{\tilde{q}}n_{\chi}-n^{\mathrm{eq}}_{\tilde{q},\mathrm{w}}n^{\mathrm{eq}}_{\chi}\right).\end{aligned} \tag{30}$$

The corresponding relations for the CP-conjugate processes are obtained analogously. In particular,

$$n^{\mathrm{eq}}_{\tilde{q}^*,\mathrm{w}}\equiv n^{\mathrm{eq}}_{\tilde{q}^*,\mathrm{w/o}}e^{-\mu_q/T}, \tag{31}$$

and hence

$$Y^{\mathrm{eq}}_{\tilde{q}^*,\mathrm{w}}\equiv Y^{\mathrm{eq}}_{\tilde{q}^*,\mathrm{w/o}}e^{-\mu_q/T}. \tag{32}$$

Since

$$Y^{\mathrm{eq}}_{\tilde{q}^*,\mathrm{w/o}}=Y^{\mathrm{eq}}_{\tilde{q},\mathrm{w/o}}, \tag{33}$$

the two effective equilibrium abundances differ only in the sign of the quark chemical potential. By CP invariance, the corresponding interaction rates satisfy

$$\begin{aligned}\langle\Gamma\rangle_{\tilde{q}^*g\to\tilde{q}\chi}&=\langle\Gamma\rangle_{\tilde{q}g\to q\chi},\\\langle\Gamma\rangle_{\tilde{q}^*\to\chi\bar{q}}&=\langle\Gamma\rangle_{\tilde{q}\to\chi q},\\\langle\Gamma\rangle_{\bar{q}^*q\to g\chi}&=\langle\Gamma\rangle_{\tilde{q}\bar{q}\to g\chi},\\\langle\sigma v\rangle_{\tilde{q}^*\chi\to\bar{q}g}&=\langle\sigma v\rangle_{\tilde{q}\chi\to qg}.\end{aligned} \tag{34}$$

By combining the decay and scattering contributions, we define the generalized conversion rates

$$\begin{aligned}\langle\Gamma\rangle_{\tilde{q}\to\chi}&\equiv\langle\Gamma\rangle_{\tilde{q}\to\chi\mathrm{SM}}+\langle\Gamma\rangle_{\tilde{q}g\to q\chi}+\langle\Gamma\rangle_{\tilde{q}\bar{q}\to g\chi}e^{-\mu_q/T},\\\langle\Gamma\rangle_{\tilde{q}^*\to\chi}&\equiv\langle\Gamma\rangle_{\tilde{q}\to\chi\mathrm{SM}}+\langle\Gamma\rangle_{\tilde{q}g\to q\chi}+\langle\Gamma\rangle_{\tilde{q}\bar{q}\to g\chi}e^{+\mu_q/T}.\end{aligned} \tag{35}$$

For $\tilde{q}\tilde{q}^*$ pair-annihilation processes, detailed balance requires

$$\langle\sigma v\rangle_{\tilde{q}\tilde{q}^*\to X\bar{X}}n^{\mathrm{eq}}_{\tilde{q},\mathrm{w/o}}n^{\mathrm{eq}}_{\tilde{q}^*,\mathrm{w/o}}=\langle\sigma v\rangle_{X\bar{X}\to\tilde{q}\tilde{q}^*}n^{\mathrm{eq}}_{X,\mathrm{w/o}}n^{\mathrm{eq}}_{\bar{X},\mathrm{w/o}}, \tag{36}$$

where $X\bar{X}$ denotes either gg or $q\bar{q}$. The corresponding collision term can therefore be written as

$$\begin{aligned}&\langle\sigma v\rangle_{\tilde{q}\tilde{q}^*\to X\bar{X}}n_{\tilde{q}}n_{\tilde{q}^*}-\langle\sigma v\rangle_{X\bar{X}\to\tilde{q}\tilde{q}^*}n_{X}n_{\bar{X}}\\&=\langle\sigma v\rangle_{\tilde{q}\tilde{q}^*\to X\bar{X}}\left[n_{\tilde{q}}n_{\tilde{q}^*}-n^{\mathrm{eq}}_{\tilde{q},\mathrm{w/o}}n^{\mathrm{eq}}_{\tilde{q}^*,\mathrm{w/o}}\frac{n_Xn_{\bar{X}}}{n^{\mathrm{eq}}_{X,\mathrm{w/o}}n^{\mathrm{eq}}_{\bar{X},\mathrm{w/o}}}\right]\\&=\langle\sigma v\rangle_{\tilde{q}\tilde{q}^*\to X\bar{X}}\left[n_{\tilde{q}}n_{\tilde{q}^*}-n^{\mathrm{eq}}_{\tilde{q},\mathrm{w/o}}n^{\mathrm{eq}}_{\tilde{q}^*,\mathrm{w/o}}\right].\end{aligned} \tag{37}$$

In the final step, we used the fact that the SM bath remains in local thermal equilibrium. For a particle–antiparticle pair, the chemical-potential factors cancel, so that

$$\frac{n_Xn_{\bar{X}}}{n^{\mathrm{eq}}_{X,\mathrm{w/o}}n^{\mathrm{eq}}_{\bar{X},\mathrm{w/o}}}=1. \tag{38}$$

Thus, the QCD pair-annihilation collision term is independent of the SM chemical potential. It contributes equally to the evolution of $Y_{\tilde{q}}$ and $Y_{\tilde{q}^*}$ and therefore cancels in their difference, leaving the net asymmetry Y_Δ unchanged. Consequently, it affects only the total partner abundance Y_Σ.

In addition to the tree-level processes $\tilde{q}\tilde{q}^*\to gg$ and $\tilde{q}\tilde{q}^*\to q\bar{q}$, which provide the dominant $2\to2$ pair-annihilation channels, we include nonperturbative Sommer-

1) For example, when $\tilde{q}$ is a $\tilde{t}$, the conversion may proceed through the three-body decay $\tilde{t}\leftrightarrow\chi bW^+$ and four-body decays such as $\tilde{t}\leftrightarrow\chi b\bar{\tau}\nu_\tau$.

CPC Accepted

feld enhancement and bound-state effects. These effects are incorporated into the effective $\tilde{q}\tilde{q}^*$ pair-annihilation cross section $\langle\sigma v\rangle_{\tilde{q}\tilde{q}^*}$ following the method described in Ref. [36].

Finally, we specify the effective thermally averaged annihilation cross section $\langle\sigma v\rangle_{\chi\chi}$ governing the ordinary thermal freeze-out of χ. The portal interaction induces the t-channel process $\chi\chi \to q\bar{q}$, whose contribution is proportional to λ^4 and is negligible in the parameter range considered here. Instead, the ordinary thermal freeze-out of χ is assumed to be governed by the additional interactions discussed in Sec. 2.1. We therefore treat their net effect phenomenologically through $\langle\sigma v\rangle_{\chi\chi}$.

We parameterize this effective annihilation cross section using the standard partial-wave expansion,

$$\langle\sigma v\rangle_{\chi\chi} = C_s + C_p \frac{T}{m_\chi}, \tag{39}$$

where C_s and C_p denote the s-wave and p-wave coefficients, respectively.

In the numerical analysis presented in Sec. 4, we consider two representative scenarios: an s-wave-dominated case,

$$C_s = 6\times10^{-9}\ \mathrm{GeV}^{-2}, \qquad C_p = 0, \tag{40}$$

and a p-wave-dominated case,

$$C_s = 0, \qquad C_p = 3\times10^{-7}\ \mathrm{GeV}^{-2}. \tag{41}$$

Both choices are selected so that, in the absence of asymmetry transfer from $\tilde{q}$, the conventional thermal freeze-out contribution to the relic density is

$$\Omega_\chi^{\mathrm{th}} h^2 \simeq 0.04. \tag{42}$$

Thus, the conventional thermal relic provides a controlled, subdominant contribution to the dark matter abundance, while the remaining abundance is generated through the late-time transfer of the $\tilde{q}$ asymmetry to χ.

III. CHEMICAL POTENTIALS IN THE BOLTZMANN EQUATIONS

The cosmic baryon asymmetry is conventionally quantified by the baryon-to-entropy ratio

$$b \equiv \frac{n_b - n_{\bar{b}}}{s}, \tag{43}$$

with the observed value $b \simeq 9\times10^{-11}$ [1]. In our model, the complex scalar $\tilde{q}$ carries a nonzero baryon number shared with SM quarks. A self-consistent treatment of the chemical potentials is therefore required to describe the coupled evolution of $\tilde{q}$, $\tilde{q}^*$, and χ. We do not address the dynamical origin of the asymmetry; instead, we track its thermal redistribution among the relevant particle species as the universe evolves, following the framework of Ref. [50].

We define the net number density of a particle species i as

$$\Delta n_i \equiv n_i - n_{\bar{i}}. \tag{44}$$

Throughout this section, the number densities of the SM species are assumed to take their local thermal equilibrium values, characterized by the corresponding chemical potentials. The exception is the scalar partner $\tilde{q}$, whose particle and antiparticle abundances are generally out of equilibrium. Its net density,

$$\Delta n_{\tilde{q}}(T) \equiv n_{\tilde{q}}(T) - n_{\tilde{q}^*}(T), \tag{45}$$

is therefore taken directly from the Boltzmann evolution and is not replaced by an equilibrium expression.

For species in local thermal equilibrium, we use the exact Fermi–Dirac and Bose–Einstein distributions to evaluate the net number densities. The net density is given by

$$\Delta n_i(T,\mu_i) = \frac{g_i}{2\pi^2}\int_{m_i}^{\infty} E\sqrt{E^2-m_i^2}\left[\frac{1}{e^{(E-\mu_i)/T}\pm1} - \frac{1}{e^{(E+\mu_i)/T}\pm1}\right] \mathrm{d}E, \tag{46}$$

where the upper sign applies to fermions and the lower sign to bosons.

Because the conserved asymmetries in the early universe are small, the chemical potentials of the SM species remain in the regime $\mu_i/T \ll 1$. We may therefore expand Eq. (46) to first order in μ_i/T,

$$\Delta n_i(T,\mu_i) \simeq \chi_i(T)\frac{\mu_i}{T}, \tag{47}$$

where

$$\chi_i(T) \equiv \left.\frac{\partial\Delta n_i}{\partial(\mu_i/T)}\right|_{\mu_i=0} = \frac{g_i}{\pi^2}\int_{m_i}^{\infty}\frac{E\sqrt{E^2-m_i^2}\,e^{E/T}}{\left(e^{E/T}\pm1\right)^2}\mathrm{d}E. \tag{48}$$

This linear expansion is particularly useful for numerical calculations. Once the chemical-equilibrium and conservation conditions are imposed, the ratios μ_i/T can be

CPC Accepted

expressed algebraically in terms of the corresponding conserved asymmetries. The chemical-potential factors $e^{\pm\mu_i/T}$ entering the collision terms of the Boltzmann equations can then be evaluated directly at each temperature, avoiding the need to solve an additional implicit system at every integration step.

It is important to distinguish the treatment of quantum statistics in this section from that adopted in Secs. 2.2 and 2.3. Here, the full Fermi–Dirac and Bose–Einstein distributions are retained when evaluating the coefficients $\chi_i(T)$, because the relation between particle asymmetries and their chemical potentials depends on the quantum statistics of the relevant species and on their mass-to-temperature ratios. In contrast, Maxwell–Boltzmann statistics are used for the thermally averaged reaction rates and collision integrals in Secs. 2.2 and 2.3. The MB approximation allows the factors $e^{\pm\mu_i/T}$ to be factorized from the phase-space integrals, leading to a convenient form of the detailed-balance relations.

The use of different statistical treatments in these two contexts is justified by their distinct roles. In the Boltzmann equations, the MB approximation simplifies the evaluation of the reaction rates and collision terms. By contrast, the coefficients $\chi_i(T)$ introduced in this section determine the relation between the physical particle asymmetries and the corresponding chemical potentials. Since the quantum-statistical corrections to the relevant reaction rates are expected to be small in the parameter range considered here, the MB treatment provides a sufficiently accurate description of the collision terms. The full Fermi–Dirac and Bose–Einstein statistics are retained where they are relevant for determining $\chi_i(T)$. This dual approach retains the relevant quantum-statistical effects in the chemical-potential relations while keeping the collision terms in a tractable MB form.

At temperatures above approximately 130 GeV, electroweak sphaleron processes are active and can redistribute baryon and lepton asymmetries among the SM particle species. Below this temperature, they become ineffective and decouple [51]. A complete treatment would require following the sphaleron-induced evolution of the relevant chemical potentials across this crossover. We do not model this dynamics explicitly. Instead, the baryon and lepton asymmetries entering the chemical-potential relations are treated as phenomenological inputs, and the sensitivity to the assumed lepton asymmetry is examined separately in Sec. 4.

The baryon asymmetry is well constrained by cosmological observations, whereas the total lepton asymmetry is comparatively weakly constrained by cosmological data [52, 53]. We therefore consider two representative choices of the lepton asymmetry. The purpose is not to model the detailed sphaleron dynamics, but to test whether the main conclusions of the asymmetry-transfer mechanism depend sensitively on the assumed lepton asymmetry.

We therefore impose the baryon and lepton asymmetries as inputs and follow their effect on the chemical potentials throughout the temperature range relevant for the Boltzmann evolution. Assuming electric charge neutrality, the relevant conservation laws are

$$l_f \equiv \frac{\Delta n_f + \Delta n_{\nu_f}}{s}, \tag{49}$$

$$b \equiv \sum_i B_i \frac{\Delta n_i}{s}, \tag{50}$$

$$0 = \sum_i Q_i \Delta n_i, \tag{51}$$

where $s = s(T)$ is the entropy density, $f \in \{e,\mu,\tau\}$ labels the lepton generations, B_i denotes the baryon number of species i ($+1/3$ for quarks and $\tilde{q}$, $-1/3$ for antiquarks and $\tilde{q}^*$, and 0 otherwise), and Q_i denotes the electric charge of species i in units of e.

Rapid SM interactions with rates satisfying $\Gamma \gg H$ enforce chemical-equilibrium relations among the corresponding chemical potentials. In particular, the gauge and weak interactions imply

$$\begin{aligned}
&\mu_\mu = \mu_e + \mu_{\nu_\mu} - \mu_{\nu_e}, && (e^- + \nu_\mu \leftrightarrow \mu^- + \nu_e),\\
&\mu_\tau = \mu_e + \mu_{\nu_\tau} - \mu_{\nu_e}, && (e^- + \nu_\tau \leftrightarrow \tau^- + \nu_e),\\
&\mu_d = \mu_u + \mu_e - \mu_{\nu_e}, && (u + e^- \leftrightarrow d + \nu_e),\\
&\mu_u = \mu_c = \mu_t, && (\text{CKM} - \text{mixed weak interactions}),\\
&\mu_d = \mu_s = \mu_b, && (\text{CKM} - \text{mixed weak interactions}),\\
&\mu_W = \mu_{\nu_e} - \mu_e, && (W^+ \leftrightarrow e^+ + \nu_e).
\end{aligned} \tag{52}$$

Importantly, the chemical potential of $\tilde{q}$ should generally not be identified with that of the corresponding SM quark. In the scenario considered here, the portal coupling λ is sufficiently small that the conversion processes involving $\tilde{q}$ need not be rapid compared with the Hubble expansion. We therefore do not impose $\mu_{\tilde{q}} = \mu_q$. Instead, the Boltzmann equations directly determine the evolution of $\Delta n_{\tilde{q}}(T)$, while the SM chemical potentials are obtained from the conservation laws and the SM chemical-equilibrium conditions. Thus, no independent $\mu_{\tilde{q}}$ is introduced into the chemical equilibrium system.

For definiteness, we consider the case in which $\tilde{q}$ couples to a quark flavor q and adopt flavor-universal lepton asymmetries,

$$l_e = l_\mu = l_\tau = \frac{l}{3}. \tag{53}$$

CPC Accepted

Substituting the linear relation $\Delta n_i \simeq \chi_i(T)(\mu_i/T)$ from Eq. (47) into the conservation laws yields the following system:

$$l_e s = \Delta n_e(T,\mu_e) + \Delta n_{\nu_e}(T,\mu_{\nu_e}), \tag{54}$$

$$[l_\mu s = \Delta n_\mu(T,\mu_e,\mu_{\nu_e},\mu_{\nu_\mu}) + \Delta n_{\nu_\mu}(T,\mu_{\nu_\mu}), \tag{55}$$

$$l_\tau s = \Delta n_\tau(T,\mu_e,\mu_{\nu_e},\mu_{\nu_\tau}) + \Delta n_{\nu_\tau}(T,\mu_{\nu_\tau}), \tag{56}$$

$$\begin{aligned} 3bs = {} & \Delta n_u(T,\mu_u) + \Delta n_d(T,\mu_u,\mu_e,\mu_{\nu_e}) + \Delta n_c(T,\mu_u) \\ & + \Delta n_s(T,\mu_u,\mu_e,\mu_{\nu_e}) + \Delta n_t(T,\mu_u) \\ & + \Delta n_b(T,\mu_u,\mu_e,\mu_{\nu_e}) + \Delta n_{\tilde{q}}(T), \end{aligned} \tag{57}$$

$$\begin{aligned} 0 = {} & \frac{2}{3}\left[\Delta n_u(T,\mu_u) + \Delta n_c(T,\mu_u) + \Delta n_t(T,\mu_u)\right] \\ & -\frac{1}{3}\Big[\Delta n_d(T,\mu_u,\mu_e,\mu_{\nu_e}) + \Delta n_s(T,\mu_u,\mu_e,\mu_{\nu_e}) \\ & +\Delta n_b(T,\mu_u,\mu_e,\mu_{\nu_e})\Big] - \Delta n_e(T,\mu_e) \\ & -\Delta n_\mu(T,\mu_e,\mu_{\nu_e},\mu_{\nu_\mu}) - \Delta n_\tau(T,\mu_e,\mu_{\nu_e},\mu_{\nu_\tau}) \\ & +\Delta n_W(T,\mu_e,\mu_{\nu_e}) + Q_{\tilde{q}}\Delta n_{\tilde{q}}(T). \end{aligned} \tag{58}$$

Here,

$$\Delta n_W \equiv n_{W^+} - n_{W^-}, \tag{59}$$

and $Q_{\tilde{q}}$ denotes the electric charge of $\tilde{q}$, expressed in units of e. Specifically,

$$Q_{\tilde{q}} = \begin{cases} +2/3, & \tilde{q} \text{ couples to an up-type quark,} \\ -1/3, & \tilde{q} \text{ couples to a down-type quark.} \end{cases} \tag{60}$$

The preceding equations constitute a closed linear system for the five independent SM chemical potentials,

$$\left\{\mu_u, \mu_e, \mu_{\nu_e}, \mu_{\nu_\mu}, \mu_{\nu_\tau}\right\}, \tag{61}$$

at each temperature T.

We briefly summarize how Eqs. (49)–(58) close this system. The SM chemical-equilibrium relations in Eq. (52), enforced by rapid gauge and weak interactions, reduce the number of independent chemical potentials to the five quantities specified above. Eqs. (49) and (50) define the lepton asymmetry l_f for each flavor and the baryon asymmetry b, respectively; these quantities are held fixed at their input values throughout the temperature evolution. Eq. (51) imposes electric charge neutrality. Together with the SM chemical-equilibrium relations, these conditions yield five independent linear equations for the five unknown chemical potentials, as given explicitly in Eqs. (54)–(58). The partner asymmetry $\Delta n_{\tilde{q}}(T)$ enters this system in two ways: through its baryon-number contribution in Eq. (57), because b is held fixed while $\Delta n_{\tilde{q}}(T)$ evolves dynamically, and through its electric-charge contribution, $Q_{\tilde{q}}\Delta n_{\tilde{q}}(T)$, in Eq. (58). Crucially, $\Delta n_{\tilde{q}}(T)$ is not determined by assuming chemical equilibrium between $\tilde{q}$ and the SM quark bath; instead, it is taken directly from the coupled Boltzmann equations, Eqs. (11)–(13), at the corresponding temperature. Since all SM asymmetries are linearized in μ_i/T via Eq. (47), this system is linear in b, l, and $Y_\Delta = \Delta n_{\tilde{q}}/s$, and can be solved algebraically at each T.

Solving this system gives the chemical potential relevant for the conversion processes in Sec. 2.3 in the form

$$\frac{\mu_q}{T} = A_q(T)\, b + B_q(T)\, l + C_q(T)\, Y_\Delta, \tag{62}$$

where

$$Y_\Delta = \frac{\Delta n_{\tilde{q}}(T)}{s} = Y_{\tilde{q}} - Y_{\tilde{q}^*}. \tag{63}$$

Here, μ_q denotes the chemical potential of the quark flavor to which $\tilde{q}$ couples. Specifically, $\mu_q = \mu_u$ when $\tilde{q}$ couples to an up-type quark, whereas $\mu_q = \mu_d$ when it couples to a down-type quark. The coefficients $A_q(T)$, $B_q(T)$, and $C_q(T)$ are dimensionless, temperature-dependent functions determined algebraically by the conservation laws above. They incorporate the temperature dependence of the coefficients $\chi_i(T)$ and, consequently, the effects associated with the relevant mass-to-temperature ratios.

Equation (62) provides the required closure for the Boltzmann system. Specifically, the chemical-potential factors that appear in the effective equilibrium abundances introduced in Sec. 2.3,

$$Y^{\rm eq}_{\tilde{q},{\rm w}} = Y^{\rm eq}_{\tilde{q},{\rm w/o}} e^{+\mu_q/T}, \qquad Y^{\rm eq}_{\tilde{q}^*,{\rm w}} = Y^{\rm eq}_{\tilde{q}^*,{\rm w/o}} e^{-\mu_q/T}, \tag{64}$$

can now be evaluated directly from b, l, Y_Δ, and the temperature T.

For the baseline numerical analysis, we take the baryon asymmetry to be

$$b = 9\times 10^{-11}. \tag{65}$$

CPC Accepted

As a benchmark scenario with a lepton asymmetry comparable to the baryon asymmetry, we adopt

$$l = -b. \tag{66}$$

To investigate the sensitivity to a substantially larger lepton asymmetry, we also consider

$$l_e = l_\mu = l_\tau = 10^{-4}, \qquad l = 3\times10^{-4}, \tag{67}$$

following the treatment of Ref. [50]. The quantitative impact of these two choices on the asymmetry-transfer mechanism is discussed in Sec. 4.

IV. NUMERICAL RESULTS

We now turn to the numerical evolution of the coupled Boltzmann equations derived in Sec. 2.3. Our main goal is to explicitly demonstrate the asymmetry-transfer mechanism illustrated schematically in Fig. 1 and to identify the region of parameter space in which the pre-existing asymmetry stored in the partner sector contributes significantly to the dark matter relic abundance.

Throughout this section, we take

$$b = 9\times10^{-11}, \tag{68}$$

and use the two representative values of the lepton asymmetry introduced in Sec. 3,

$$l = -b \tag{69}$$

and

$$l = 3\times10^{-4}. \tag{70}$$

Comparing these two choices provides a robustness test of the asymmetry-transfer mechanism with respect to the assumed lepton asymmetry.

For the benchmark evolution plots, we consider a stop-like partner $\tilde{q} = \tilde{t}$ with

$$m_{\tilde{q}} = 2\ \text{TeV}, \qquad m_\chi = 500\ \text{GeV}, \tag{71}$$

and use the s-wave-dominated effective $\chi\chi$ annihilation cross section

$$C_s = 6\times10^{-9}\ \text{GeV}^{-2}, \qquad C_p = 0. \tag{72}$$

In the absence of asymmetry transfer, these parameters yield

$$\Omega_\chi h^2 \simeq 0.04, \tag{73}$$

such that the conventional thermal relic abundance of χ provides only a subdominant contribution to the observed dark matter abundance.

A. Benchmark evolution and the asymmetry-transfer mechanism

We first consider

$$\lambda = 2.5\times10^{-9}, \tag{74}$$

for which the final dark matter abundance is near the observed value. The corresponding evolution of the relevant yields and interaction rates is shown in Fig. 2.

The benchmark evolution illustrates the three main stages underlying the asymmetry-transfer mechanism in Fig. 1. At early times, both χ and $\tilde{q}$ are in thermal equilibrium, and the primordial asymmetry is shared between the SM quark and partner sectors. Subsequent QCD annihilation of $\tilde{q}\tilde{q}^*$ efficiently removes the particle-antiparticle symmetric component of the partner population. Because these annihilations involve one $\tilde{q}$ and one $\tilde{q}^*$, they do not directly change the net asymmetry.

$$Y_\Delta = Y_{\tilde{q}} - Y_{\tilde{q}^*}. \tag{75}$$

Consequently, once the symmetric component has been depleted, the remaining partner abundance is increasingly dominated by the asymmetric component.

For the benchmark masses, depletion of the symmetric partner population occurs around

$$\frac{m_{\tilde{q}}}{T} \sim 25, \qquad x \sim 6. \tag{76}$$

At early times, the conversion processes are too inefficient to maintain chemical equilibrium between $\tilde{q}$ and χ. As the Universe evolves, the ratio of the relevant conversion rates to the Hubble expansion rate changes, and the conversion processes eventually become dynamically important. For the benchmark point, this occurs after the ordinary thermal freeze-out of χ has taken place. The subsequent conversion therefore transfers part of the asymmetry stored in the $\tilde{q}$ sector to χ, with the decay $\tilde{q}\to\chi q$ providing the dominant contribution.

The conversion processes therefore do not simply maintain chemical equilibrium between $\tilde{q}$ and χ throughout the evolution. Instead, their time-dependent efficiency determines how much of the asymmetry stored

CPC Accepted

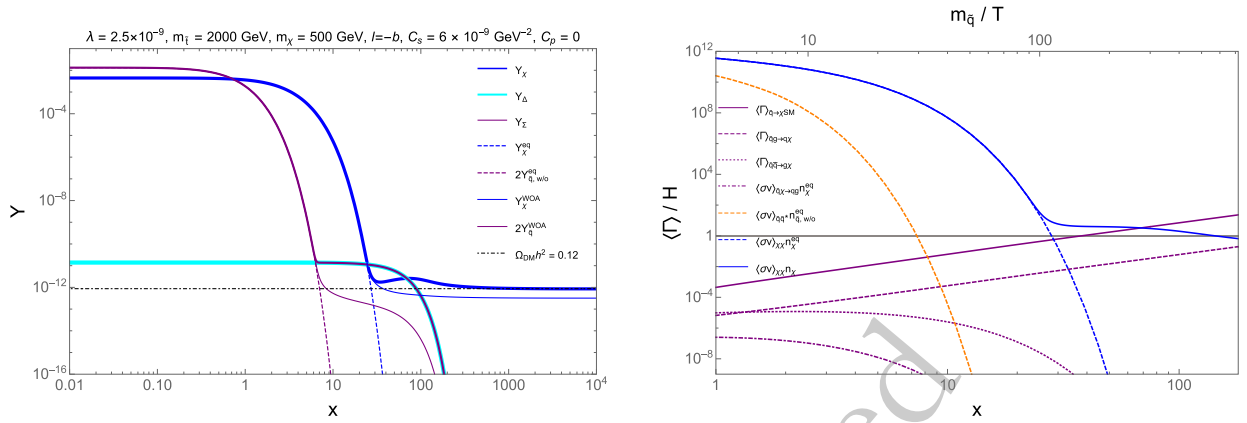

Fig. 2. (color online) Evolution of the particle abundances and interaction rates for the benchmark parameter choice $m_{\tilde{q}} = 2$ TeV, $m_\chi = 500$ GeV, $\lambda = 2.5\times10^{-9}$, $l = -b$, $C_s = 6\times10^{-9}$ GeV^{-2}, and $C_p = 0$. Left panel: the yields Y_χ, Y_Σ, and Y_Δ obtained from the coupled Boltzmann equations, together with the corresponding equilibrium and "without asymmetry" results (labeled "WOA"). The WOA results are obtained by setting $\mu_q = 0$ and $Y_\Delta = 0$ when solving Eqs. (11) and (12). The horizontal dot-dashed line indicates the observed dark matter abundance, $\Omega_{\rm DM}h^2 = 0.12$. Right panel: the relevant thermally averaged interaction rates divided by the Hubble expansion rate as functions of $x = m_\chi/T$. The upper axis indicates the corresponding value of $m_{\tilde{q}}/T$.

in the partner reservoir is transferred to χ and, more importantly, when this transfer occurs relative to the freeze-out of χ.

As the asymmetry is transferred, Y_χ temporarily increases above the would-be thermal relic trajectory. The newly produced χ particles can still annihilate efficiently during part of this period, leading to a subsequent decrease in Y_χ. The final relic abundance is therefore determined by the competition between the late-time injection of χ from the surviving partner asymmetry and the residual $\chi\chi$ annihilation rate.

This behavior provides a direct numerical realization of the conceptual picture in Fig. 1: QCD annihilations first remove the symmetric component of the partner population while preserving its net asymmetry. The surviving asymmetric component is subsequently transferred to χ at relatively late times, after the ordinary thermal freeze-out of χ. Consequently, the final dark matter abundance is controlled by both the amount of asymmetry that survives in the partner sector and the efficiency with which the injected χ particles annihilate after the transfer.

B. Dependence on the portal coupling

The portal coupling controls the timing of the transfer of the partner asymmetry to χ. Since the conversion rates scale approximately as λ^2, varying λ changes the relative timing of asymmetry transfer and the ordinary thermal freeze-out of χ.

For a larger coupling,

$$\lambda = 2.5\times10^{-8}, \tag{77}$$

the conversion processes become effective at an earlier stage of the evolution. As a result, the partner-sector

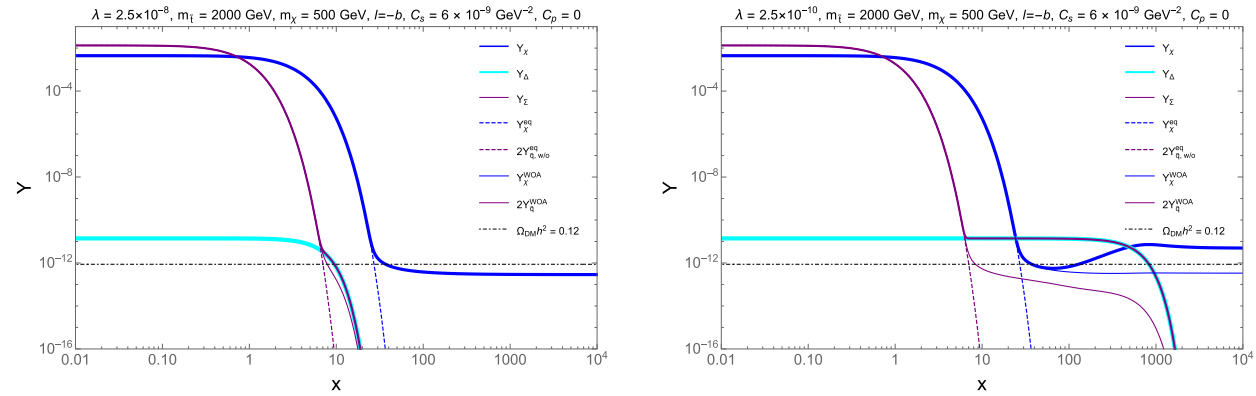

Fig. 3. (color online) Evolution of the particle abundances for the same benchmark parameters as in Fig. 2, but with $\lambda = 2.5\times10^{-8}$ (left) and $\lambda = 2.5\times10^{-10}$ (right). The larger coupling induces an earlier transfer of the partner-sector asymmetry, whereas the smaller coupling delays the transfer until the residual $\chi\chi$ annihilation becomes less efficient.

CPC Accepted

asymmetry is transferred to χ before the ordinary thermal freeze-out of χ is completed. The χ particles produced through this early transfer can still annihilate efficiently, so the transferred component does not make a significant additional contribution to the final dark matter abundance. The relic density therefore remains close to that obtained from the ordinary thermal freeze-out of χ alone.

Conversely, for

$$\lambda = 2.5\times10^{-10}, \tag{78}$$

the weaker portal interaction delays the transfer of the partner-sector asymmetry. Consequently, a larger fraction of the surviving asymmetry is transferred to χ only at later times, when the $\chi\chi$ annihilation rate has already become substantially smaller than the Hubble rate. The newly produced χ particles are therefore annihilated less efficiently, resulting in a larger final relic abundance.

These three cases illustrate the characteristic dependence of the final relic abundance on the timing of asymmetry transfer:

$$\lambda \text{ too large} \implies \text{transfer too early}, \tag{79}$$

$$\lambda \text{ intermediate} \implies \text{transfer during the relevant freeze}-\text{out epoch}, \tag{80}$$

and

$$\lambda \text{ too small} \implies \text{transfer too late}. \tag{81}$$

If transfer occurs early, the injected χ particles are efficiently annihilated, whereas if transfer occurs sufficiently late, the annihilation efficiency is too low to remove the injected population. An intermediate portal coupling therefore allows the asymmetry to be transferred at a time when its contribution to the final relic abundance can be significant and can reproduce the observed value.

For the benchmark mass choice, a scan over λ confirms this qualitative picture, as shown in the left panel of Fig. 4. For $\lambda \gtrsim 10^{-8}$, the asymmetry-transfer contribution becomes negligible, whereas for sufficiently small λ, the transferred asymmetry can lead to an overabundance.

For even smaller couplings, late transfer is accompanied by an increasingly long partner lifetime, and cosmological constraints on long-lived colored particles become relevant. In particular, requiring the partner to decay before Big Bang nucleosynthesis (BBN) [54–56] gives a characteristic lower bound of order $\lambda \gtrsim 10^{-13}$ for the benchmark considered here. For the benchmark value $\lambda = 2.5\times10^{-9}$, the partner lifetime is only about 3 ns, so the $\tilde{q}$ population decays before the quark–hadron transition and does not produce a cosmologically relevant population of R-hadrons. For the benchmark masses, the parameter space with $\lambda \lesssim 10^{-13}$ already yields a dark matter relic abundance well above the observed value.

The right panel of Fig. 4 shows the dependence of the final relic abundance on m_χ, with $\lambda = 2.5\times10^{-9}$ and $m_{\tilde{q}} = 2$ TeV fixed. The relic abundance generally increases as m_χ increases. The two representative choices of the lepton asymmetry exhibit similar overall behavior, although their numerical values differ because of the different quark chemical potentials entering the conversion terms.

For the stop-like benchmark, an additional feature appears when

$$m_{\tilde{t}} - m_\chi < m_t, \tag{82}$$

at which the two-body decay $\tilde{t} \to \chi t$ becomes kinematic-

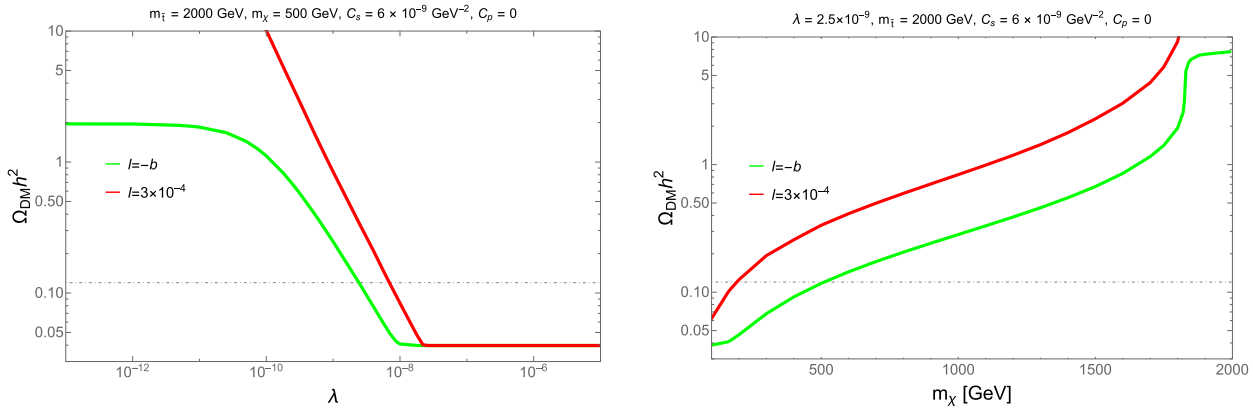

Fig. 4. (color online) Final dark matter relic abundance $\Omega_{\rm DM}h^2$ as a function of the portal coupling λ (left panel) and the dark matter mass m_χ (right panel), with fixed $m_{\tilde{q}} = 2$ TeV. The green and red curves correspond to $l = -b$ and $l = 3\times10^{-4}$, respectively. The remaining parameters are those of the benchmark shown in Fig. 2. The horizontal line indicates the observed value, $\Omega_{\rm DM}h^2 \simeq 0.12$.

CPC Accepted

ally forbidden. The relic-density curve changes more rapidly near this threshold because the dominant conversion channel changes; scattering and higher-body decay processes become increasingly important. As m_χ approaches $m_{\tilde{t}}$, the phase space available for conversion processes is further reduced, and the relic abundance approaches limiting behavior.

C. Dependence on the mass hierarchy

The dependence on m_χ displayed in the right panel of Fig. 4 reflects the interplay between the mass hierarchy and the timing of asymmetry transfer. We therefore examine this dependence more directly by varying m_χ while keeping

$$m_{\tilde{q}} = 2\ \text{TeV}, \qquad \lambda = 2.5\times10^{-9}, \tag{83}$$

fixed.

As m_χ increases toward $m_{\tilde{q}}$, the relative timing of the conversion process and χ freeze-out changes, and the surviving partner asymmetry can be transferred at larger values of $x = m_\chi/T$. At these later times, residual $\chi\chi$ annihilation is less efficient, enhancing the contribution of the transferred asymmetry to the final relic density.

For substantially smaller m_χ, the hierarchy

$$m_{\tilde{q}} \gg m_\chi \tag{84}$$

more strongly separates the QCD-driven depletion of the partner population, the conversion of the surviving asymmetry, and the standard freeze-out of χ. In this regime, asymmetry transfer can occur sufficiently early that a large fraction of the resulting χ population is subsequently annihilated, reducing its contribution to the final relic abundance.

The key point is that the mechanism does not require a compressed spectrum. In contrast to standard coannihilation, the relevant reservoir is the surviving asymmetric component rather than the thermally suppressed symmetric abundance of the heavier state. Thus, a substantial mass hierarchy can remain compatible with efficient asymmetry transfer, provided that the conversion history is appropriately arranged.

More generally, the relic abundance depends on both the mass hierarchy and the portal coupling. Consequently, different combinations of $(\lambda, m_{\tilde{q}}, m_\chi)$ can yield the same observed dark matter abundance, as illustrated by the contour in Fig. 6.

The benchmark results presented above were obtained primarily for $m_{\tilde{t}} = 2$ TeV. To illustrate the behavior for a different partner mass, we also consider

$$m_{\tilde{t}} = 3\ \text{TeV}. \tag{85}$$

For $l = -b$ and $\langle\sigma v\rangle_{\chi\chi} = 6\times10^{-9}\ \text{GeV}^{-2}$, suitable choices of the portal coupling and dark matter mass can also reproduce the observed relic abundance. For example,

$$(\lambda, m_{\tilde{t}}, m_\chi) = (1.8\times10^{-9},\ 3\ \text{TeV},\ 480\ \text{GeV}) \tag{86}$$

and

$$(\lambda, m_{\tilde{t}}, m_\chi) = (1.0\times10^{-8},\ 3\ \text{TeV},\ 1.6\ \text{TeV}) \tag{87}$$

both give

$$\Omega_\chi h^2 \simeq 0.12. \tag{88}$$

These examples demonstrate that the asymmetry-transfer mechanism can remain viable for different partner masses, with the portal coupling and dark matter mass adjusted accordingly.

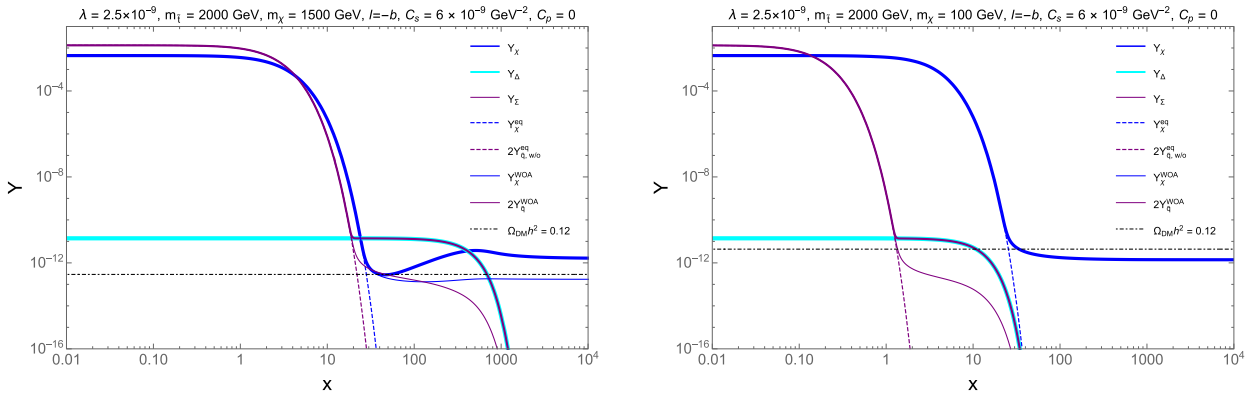

Fig. 5. (color online) Evolution of the particle abundances for $m_\chi = 1.5$TeV (left) and $m_\chi = 100$GeV (right), with $m_{\tilde{q}} = 2$TeV and $\lambda = 2.5\times10^{-9}$. All other parameters are the same as in Fig. 2. This comparison illustrates how the mass hierarchy determines the relative timing of asymmetry transfer and χ freeze-out.

CPC Accepted

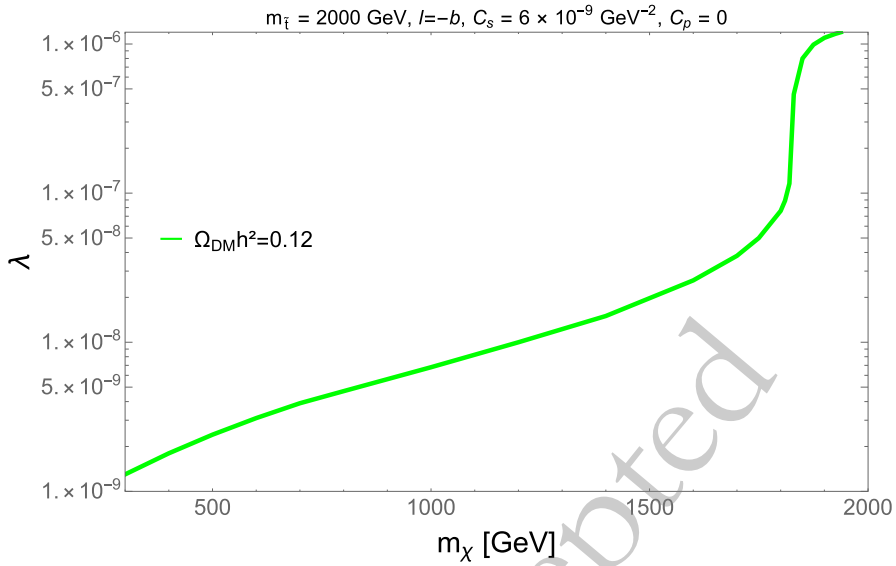

Fig. 6. (color online) Parameter combinations in the (m_χ, λ) plane that yield $\Omega_{\rm DM}h^2 \simeq 0.12$ for fixed $m_{\tilde{q}} = 2$ TeV, $l = -b$, and the benchmark s-wave annihilation cross section. The curve illustrates the degeneracy between the portal coupling and the dark matter mass in reproducing the observed relic abundance.

D. Near-degenerate spectra

In the hierarchical parameter region relevant to the main asymmetry-transfer mechanism, we typically consider $\lambda \lesssim 10^{-8}$. Near-degenerate spectra can remain viable for larger portal couplings, for which additional conversion channels become relevant. For a stop-like partner, this region exhibits an additional kinematic feature: the two-body decay $\tilde{t} \to \chi t$ becomes kinematically forbidden when $m_{\tilde{t}} - m_\chi < m_t$. The conversion dynamics is then governed by scattering processes and higher-body decays rather than by the two-body decay alone. The available phase space becomes increasingly suppressed as $m_{\tilde{t}} - m_\chi$ decreases, leading to a rapidly increasing partner lifetime. The resulting long lifetime is also a familiar feature of highly degenerate spectra in coannihilation-type scenarios.

In this regime, the conversion history can include more than one stage. Scattering processes involving thermal top quarks become relevant at early times but are rapidly suppressed as the temperature decreases, owing both to the top-quark mass and to the limited available phase space. Higher-multiplicity decay channels can then become important at later times. The remaining partner asymmetry is consequently transferred in multiple stages, with part of the asymmetry converted before χ freeze-out and the remainder transferred later. This near-degenerate regime is therefore qualitatively distinct from the small-λ hierarchical regime discussed above.

This example demonstrates that the asymmetry-transfer mechanism is not restricted to a single dominant microscopic conversion channel. The relevant requirement is instead that the total conversion history leaves an appropriate fraction of the partner-sector asymmetry to be transferred at a time when it can contribute to the final χ abundance.

E. Dependence on the dark matter annihilation mode

The final relic abundance is sensitive to the annihilation properties of χ when the asymmetry transfer occurs after, or near, the ordinary thermal freeze-out of χ. In this case, the injected χ particles are no longer efficiently driven back toward chemical equilibrium, and their persistence in the dark matter sector depends on the $\chi\chi$ annihilation rate at the time of injection. Consequently, the relic abundance can depend sensitively on whether the annihilation is dominated by s-wave or p-wave processes.

By contrast, if the asymmetry is transferred sufficiently early, before χ freeze-out, the injected χ particles can still annihilate efficiently and track the thermal abundance. In this regime, the final relic density is much less sensitive to the detailed annihilation mode.

We compare the benchmark s-wave case,

$$C_s = 6\times10^{-9}\ \mathrm{GeV}^{-2}, \qquad C_p = 0, \tag{89}$$

with a representative p-wave case shown in the left panel of Fig. 8,

$$C_s = 0, \qquad C_p = 3\times10^{-7}\ \mathrm{GeV}^{-2}. \tag{90}$$

The qualitative evolution in the p-wave case is the same as that in the benchmark s-wave scenario: the symmetric partner population is first depleted, leaving a residual asymmetry in Y_Δ, which is subsequently transferred to χ. The main difference is that the p-wave annihilation

CPC Accepted

cross section decreases with temperature,

$$\langle\sigma v\rangle_{\chi\chi} \simeq C_p \frac{T}{m_\chi}, \tag{91}$$

so that the annihilation of newly produced χ particles becomes less efficient at late times. Consequently, the post-transfer decrease in Y_χ is milder, and the final relic abundance is larger.

For the representative benchmark, the p-wave choice gives $\Omega_{\rm DM}h^2 \simeq 0.27$, compared with $\Omega_{\rm DM}h^2 \simeq 0.12$ for the s-wave choice. This difference does not indicate a qualitatively different asymmetry-transfer mechanism. Rather, it reflects the different annihilation efficiencies of the injected χ population at the time of transfer.

F. Sensitivity to the lepton asymmetry

We finally examine how the results depend on the lepton asymmetry. As discussed in Sec. 3, we do not explicitly model the sphaleron-induced redistribution of asymmetries. Instead, the two choices of l are used as representative inputs to assess the sensitivity of the asymmetry-transfer mechanism to the lepton asymmetry.

The corresponding relic-density curves are shown in Fig. 4. The larger lepton asymmetry induces a different quark chemical potential through the conservation equations, thereby modifying the effective equilibrium abundances that enter the conversion terms. This can affect the detailed evolution of Y_Δ and Y_χ, as illustrated in the right panel of Fig. 8. Nevertheless, the overall behavior remains qualitatively unchanged: the symmetric partner population is depleted by QCD annihilations, a surviving asymmetric component remains in the partner sector, and this asymmetry is subsequently transferred to χ.

For the larger lepton asymmetry, the magnitude of μ_q/T is enhanced relative to the $l=-b$ benchmark, while

CPC Accepted

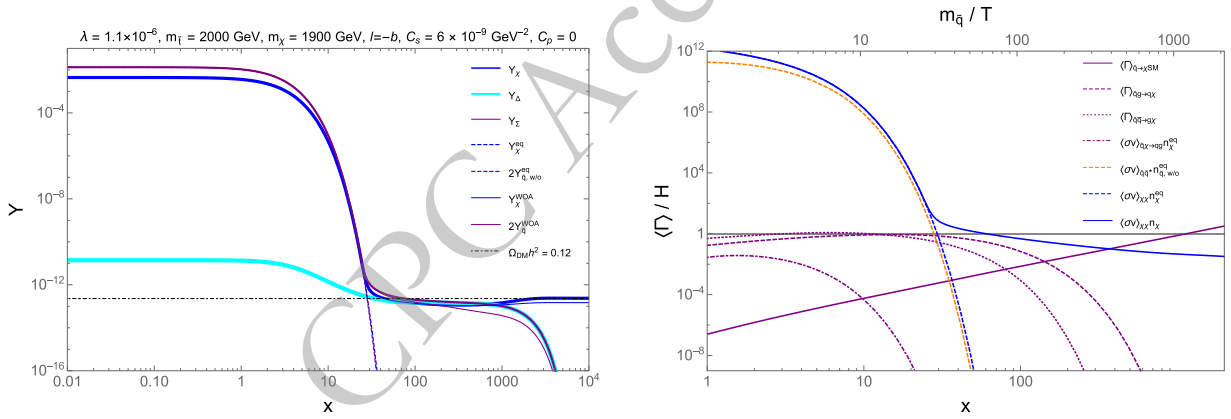

Fig. 7. (color online) Near-degenerate mass spectrum for $m_{\tilde{t}} = 2$TeV, $m_\chi = 1.9$TeV, and $\lambda = 1.1\times10^{-6}$. Left panel: evolution of the particle abundances. Right panel: corresponding conversion and annihilation rates normalized to the Hubble expansion rate. Because the two-body decay $\tilde{t}\to\chi t$ is kinematically forbidden, conversion proceeds through scattering processes at early times and through multibody decays at later times.

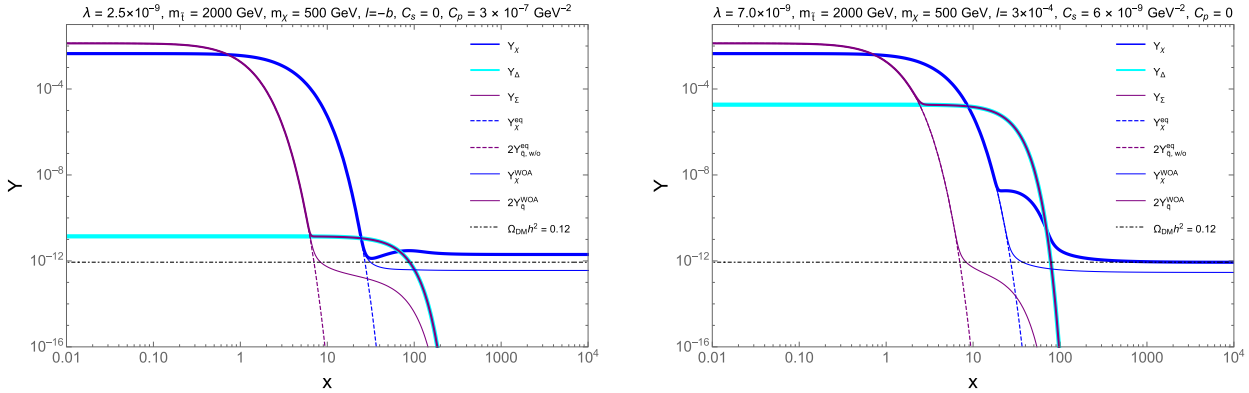

Fig. 8. (color online) Left panel: evolution for the p-wave-dominated annihilation choice $C_s = 0$ and $C_p = 3\times10^{-7}$ GeV^{-2}, with the remaining parameters set equal to those in Fig. 2. Right panel: evolution for the benchmark s-wave annihilation choice, but with the larger lepton asymmetry $l = 3\times10^{-4}$. The comparison illustrates the effects of the late-time $\chi\chi$ annihilation rate and the chemical-potential dependence of the asymmetry-transfer process.

remaining within the range in which the linearized treatment of the chemical potentials adopted in Sec. 3 is applicable. The resulting relic-density curve can therefore differ quantitatively from the $l=-b$ case, but it retains the same characteristic dependence on λ and the same qualitative transition between asymmetry-transfer-dominated and thermally dominated relic abundance.

The two choices of l should therefore be interpreted as a robustness test rather than as two explicitly modeled cosmological histories. The persistence of the same qualitative intermediate-coupling regime indicates that the central asymmetry-transfer mechanism is not sensitive to the precise value of the lepton asymmetry.

G. Summary of the numerical picture

The numerical results can be summarized by the following physical picture. The partner sector initially contains both symmetric and asymmetric populations. QCD annihilations efficiently deplete the symmetric component, reducing Y_Σ while leaving the net partner asymmetry Y_Δ essentially unchanged. At later times, the surviving asymmetric component is transferred to χ through the portal interaction.

$$Y_\Delta \longrightarrow Y_\chi. \tag{92}$$

The final dark matter abundance is therefore governed by three interrelated factors:

1. the magnitude of the asymmetry that survives QCD depletion and early conversion;

2. the time at which the remaining asymmetry is transferred to χ; and

3. the efficiency of $\chi\chi$ annihilation following the transfer.

This behavior explains the characteristic dependence on the portal coupling. For large λ, the asymmetry is transferred at too early a stage, and the resulting χ population is largely depleted by annihilations before it can contribute to the frozen dark matter abundance. For very small λ, the transfer occurs too late, after $\chi\chi$ annihilation has become inefficient, resulting in an overabundance. An intermediate range of λ allows the transfer to occur when a substantial fraction of the injected χ population can survive, making it possible to reproduce the observed relic abundance.

The same picture also explains why a compressed mass spectrum is not required. The relevant reservoir is the asymmetric component of the partner population, rather than its thermally suppressed symmetric abundance. Consequently, hierarchical spectra with $m_{\tilde{q}} \gg m_\chi$ can remain viable.

The comparison of the two representative lepton asymmetries shows that the detailed chemical-potential evolution can modify the numerical results without changing the basic mechanism. Together with the s-wave/p-wave comparison, this demonstrates that the central result is not tied to a particular annihilation mode or to a particular choice of the lepton asymmetry.

The numerical analysis therefore provides a consistent realization of the conceptual picture introduced in Fig. 1: a primordial baryon asymmetry is temporarily stored in the partner sector, the symmetric partner population is removed by QCD annihilation, and the surviving asymmetric component is subsequently transferred to the Majorana dark matter particle, thereby supplying the dominant contribution to its relic abundance.

The numerical results presented above focus on the stop-like partner $\tilde{q}=\tilde{t}$. The stop case has an additional kinematic feature associated with the relatively large top-quark mass: the two-body decay $\tilde{t}\to\chi t$ becomes kinematically forbidden for sufficiently compressed spectra, leading to a change in the dominant conversion channels, as discussed above. Apart from this kinematic feature, the asymmetry-transfer mechanism and its qualitative dependence on the portal coupling and mass hierarchy are common to other choices of the colored scalar partner. We therefore turn in the next section to the collider implications for both stop-like and sbottom-like partner scenarios. Here, these terms refer only to the corresponding gauge quantum numbers and collider phenomenology of the colored scalar mediator and do not imply a specific MSSM realization.

V. LHC constraints from long-lived particle searches

The small couplings considered in Sec. 4 can also make $\tilde{q}$ long-lived on detector length scales. For the benchmark point considered, $m_{\tilde{q}}=2000\,\mathrm{GeV}$, $m_\chi=500\,\mathrm{GeV}$, and $\lambda=2.5\times10^{-9}$, the lifetime of $\tilde{q}$ is approximately 3 ns, corresponding to a proper decay length of $c\tau_{\tilde{q}}\simeq 1\,\mathrm{m}$. Such a lifetime lies in the range relevant to long-lived-particle searches at the LHC. After production at the LHC, a long-lived $\tilde{q}$ hadronizes into an R-hadron, whose charged states can produce tracks with anomalously large ionization energy loss [32]. Such signatures are directly probed by searches for heavy long-lived charged particles at the LHC [33]. We therefore examine the corresponding constraints on both $\tilde{t}$ and $\tilde{b}$ scenarios considered in this work.

We follow the ATLAS full Run-2 large-dE/dx search and the corresponding public reinterpretation prescription. The auxiliary efficiency tables and model-independent limits are taken from the HEPData record [57]. Signal events for $pp\to\tilde{q}\tilde{q}^*$ are generated with MadGraph5_aMC@NLO [58], followed by parton showering and hadronization with Pythia 8 [59]. We use the NNLO+NNLL predictions for $\tilde{t}$ and $\tilde{b}$ pair-production cross sections from NNLL-Fast [60]. The pair-production cross sections are taken to be identical for a given

CPC Accepted

$m_{\tilde{q}}$, because $\tilde{q}\tilde{q}^*$ production is dominated by QCD interactions and electroweak contributions are subdominant. For the collider recast, we consider two representative non-compressed benchmarks with $m_\chi = 300$ GeV and 500 GeV. A detailed treatment of compressed spectra, for which the event-level acceptance can depend on the decay kinematics, is not included in the present analysis. The signal yields are compared with model-independent 95% CL limits.

The collider constraints, together with the relic-density contours, are shown in Fig. 9. The exclusion contours for the two m_χ benchmarks nearly overlap in the upper panels, indicating only a weak dependence on m_χ in the non-compressed regime considered here. This behavior is

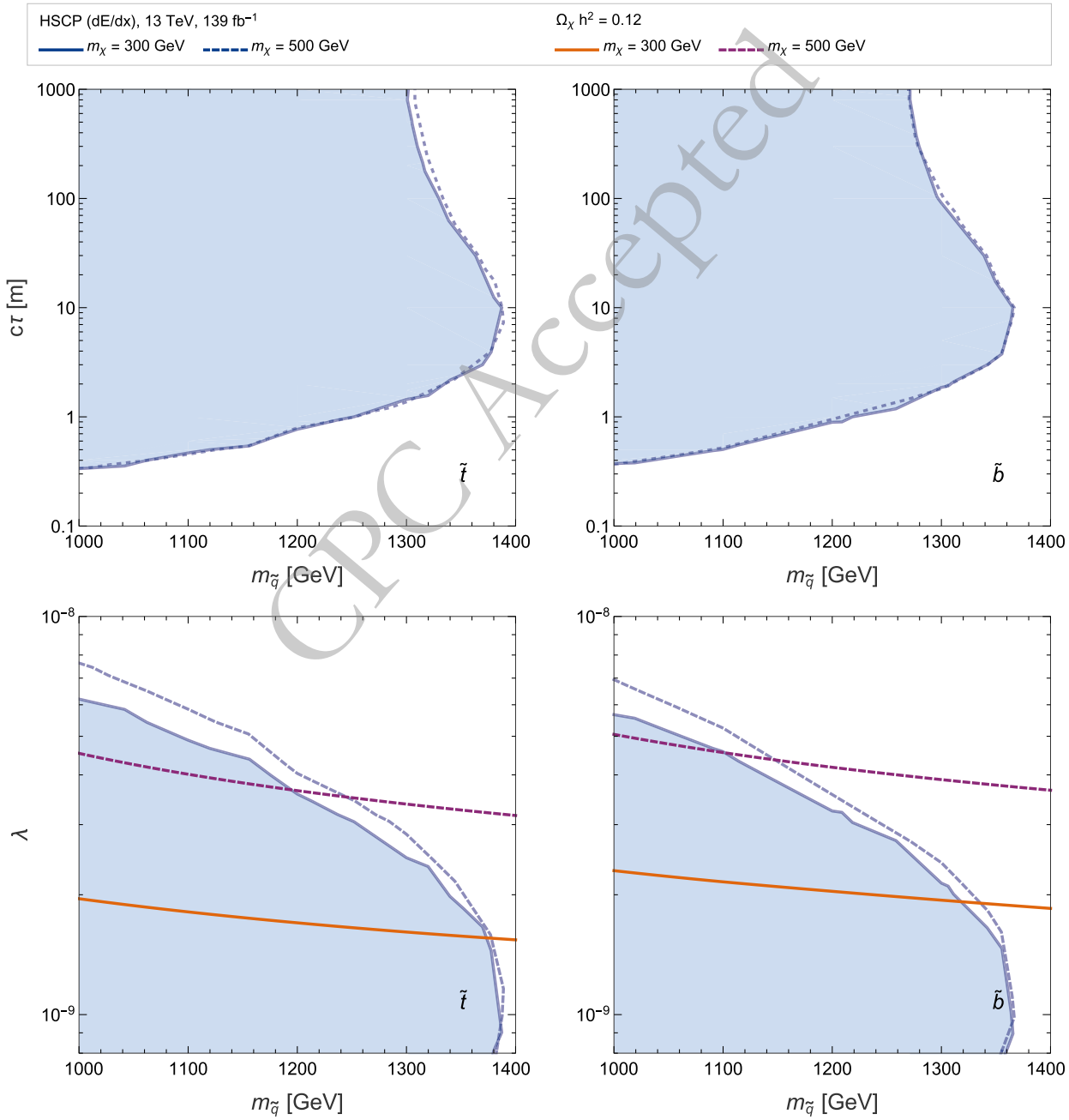

Fig. 9. (color online) Recast of the observed 95% CL exclusion regions from the ATLAS large-dE/dx HSCP search at $\sqrt{s} = 13$ TeV with 139 fb^{-1} for the $\tilde{t}$ (left) and $\tilde{b}$ (right) scenarios. The upper panels present the constraints in the $(m_{\tilde{q}}, c\tau)$ plane, and the lower panels show those in the $(m_{\tilde{q}}, \lambda)$ plane. The blue solid (dashed) curves indicate the exclusion boundaries for $m_\chi = 300$ (500) GeV, with the light-blue shading denoting the excluded region for the 300 GeV benchmark. The orange solid (purple dashed) curves in the lower panels represent the $\Omega_\chi h^2 = 0.12$ contours for $m_\chi = 300$ (500) GeV.

expected because the production rate is controlled predominantly by QCD processes and hence by $m_{\tilde{q}}$, whereas the residual dependence on m_χ enters through the decay kinematics and event-level acceptance. For the non-compressed spectra considered in this recast, and neglecting the final-state quark mass, the proper decay length can be conveniently estimated as

$$c\tau_{\tilde{q}} \simeq 1.6\ \mathrm{m}\left(\frac{\lambda}{2.5\times10^{-9}}\right)^{-2}\left(\frac{m_{\tilde{q}}}{1\ \mathrm{TeV}}\right)^{-1}\left(1-\frac{m_\chi^2}{m_{\tilde{q}}^2}\right)^{-2}. \quad (93)$$

The strongest limits are obtained when $c\tau \sim 10\ \mathrm{m}$, for which $m_{\tilde{q}}$ values up to approximately 1.4 TeV are excluded. This reflects the balance between the loss of track efficiency at shorter lifetimes and the reduced E_T^{miss} trigger efficiency in the detector-stable limit. The slight difference between the $\tilde{t}$ and $\tilde{b}$ contours mainly originates from the differing charge compositions of their R-hadrons, which lead to a somewhat larger signal acceptance in the $\tilde{t}$ case. The lower panels translate the same HSCP constraints into the $(m_{\tilde{q}},\lambda)$ plane, where they can be directly compared with the $\Omega_\chi h^2 = 0.12$ contours. The separation between the two HSCP exclusion contours mainly arises from the m_χ dependence of the two-body decay phase space.

Using $\tau_{\tilde{q}} \sim O(1\ \mathrm{s})$ as a characteristic BBN timescale gives $c\tau_{\tilde{q}} \sim 3\times10^8\ \mathrm{m}$, corresponding to the lower bound of approximately $\lambda \gtrsim 10^{-13}$ discussed in Sec. 4.2. By contrast, Fig. 9 covers $c\tau_{\tilde{q}} \lesssim 10^3\ \mathrm{m}$, or $\tau_{\tilde{q}} \lesssim 3.3\times10^{-6}\ \mathrm{s}$, with relevant couplings of order 10^{-9} or larger. The parameter region probed here is therefore well separated from the BBN-sensitive regime, and no BBN exclusion contour is shown.

At shorter decay lengths, searches targeting displaced decays can provide complementary sensitivity to the HSCP constraints considered here [30, 61]. The main cosmological benchmark, with $m_{\tilde{q}} = 2\ \mathrm{TeV}$, lies beyond the mass range constrained by the present HSCP recast. For such heavy states, searches combining ionization and time-of-flight information can improve the identification of slow R-hadrons and may further extend the sensitivity at the HL-LHC [62, 63]. A substantial extension into the multi-TeV mass range would ultimately require higher-energy hadron colliders [64].

VI. Conclusion

We have studied a mechanism in which a primordial baryon asymmetry is temporarily stored in a sector of heavier colored partners and subsequently transferred to a self-conjugate dark matter particle. In the simplified model considered here, the dark matter particle is a Majorana fermion χ, while the partner $\tilde{q}$ is a complex scalar that carries baryon number and couples to a Standard Model quark through a small portal interaction. Unlike in conventional asymmetric dark matter scenarios, the dark matter particle itself need not carry a conserved particle-antiparticle asymmetry. Instead, the partner sector acts as a temporary reservoir for the primordial asymmetry.

At early times, the partner population contains both symmetric and asymmetric components. QCD interactions efficiently deplete the symmetric component through $\tilde{q}\tilde{q}^*$ annihilation while leaving the net asymmetry, $Y_\Delta = Y_{\tilde{q}} - Y_{\tilde{q}^*}$, essentially unchanged. For sufficiently small portal couplings, the conversion processes do not maintain chemical equilibrium throughout this stage, allowing a substantial asymmetric component to survive after the symmetric population has disappeared. This surviving asymmetry can subsequently be transferred to χ through decays and scattering processes.

We have incorporated the chemical-potential dependence of the conversion processes self-consistently. The SM chemical potentials are determined by the baryon and lepton asymmetries, electric charge neutrality, and the chemical-equilibrium conditions enforced by rapid SM interactions, while the partner asymmetry Y_Δ is evolved directly using the Boltzmann equations. In particular, we do not impose $\mu_{\tilde{q}} = \mu_q$, since the small portal coupling need not maintain chemical equilibrium between the partner and the SM quark.

The numerical results demonstrate that the final dark matter abundance is determined by the interplay of three effects: the amount of asymmetry that survives the depletion of the symmetric partner population, the time at which this surviving asymmetry is transferred to χ, and the efficiency of $\chi\chi$ annihilation after the transfer. The portal coupling λ plays a central role because it controls the timing of the transfer. For large λ, the asymmetry is transferred too early, when the produced χ particles can still annihilate efficiently, leaving a relic abundance close to the ordinary thermal result. For sufficiently small λ, the transfer occurs too late, after $\chi\chi$ annihilation has become inefficient, and the transferred component can instead lead to an overabundance. An intermediate range of portal couplings therefore allows the transferred asymmetry to provide a substantial, and potentially dominant, contribution to the observed dark matter abundance.

An important feature of this mechanism is that it does not require a compressed mass spectrum. We find viable examples with a substantial hierarchy between the partner and dark matter masses, including benchmark configurations with $m_{\tilde{q}} \gg m_\chi$. In such cases, the partner abundance relevant to the mechanism is the surviving asymmetric component rather than the thermally suppressed symmetric abundance. The dependence on the mass hierarchy can nevertheless be significant because changing m_χ modifies the relative timing of partner depletion, asymmetry transfer, and dark matter freeze-out. Near-degenerate spectra exhibit additional kinematic structure,

CPC Accepted

particularly in the stop-like case, where the two-body decay $\tilde{t} \to \chi t$ can become forbidden and scattering or higher-body decay processes can dominate the conversion history.

The annihilation properties of χ provide another important source of variation. When the asymmetry is transferred after dark matter freeze-out, the final relic abundance depends sensitively on the annihilation rate at the time of injection. We therefore find a larger relic abundance for the representative p-wave benchmark than for the corresponding s-wave case, reflecting the suppression of the p-wave annihilation rate at late times. This dependence does not alter the underlying asymmetry-transfer mechanism, but it determines how much of the transferred population survives as dark matter.

We have also examined the sensitivity to the lepton asymmetry by comparing $l = -b$ with a substantially larger representative value, $l = 3 \times 10^{-4}$. The different lepton asymmetries modify the SM quark chemical potentials and consequently affect the detailed evolution of the conversion processes and the final relic density. Nevertheless, the qualitative behavior remains unchanged: QCD annihilation removes the symmetric partner population, a residual asymmetric component survives, and this component is transferred to χ at later times. This indicates that the basic mechanism is not tied to a particular choice of the lepton asymmetry, although a quantitative treatment of the sphaleron-active era would be required for a more complete description of the chemical-potential evolution.

Finally, the small portal couplings relevant for late asymmetry transfer can make the colored partner long-lived on detector scales. For the benchmark point with $m_{\tilde{t}} = 2\,\mathrm{TeV}$, $m_{\chi} = 500\,\mathrm{GeV}$, and $\lambda = 2.5 \times 10^{-9}$, the predicted lifetime is of order a few nanoseconds, corresponding to a proper decay length of order one meter. Such states can hadronize into long-lived R-hadrons and are therefore subject to searches for heavy stable or metastable charged particles. Our recast of the ATLAS Run-2 large-dE/dx search shows that existing HSCP searches constrain part of the parameter space for both stop-like and sbottom-like partners, while heavier partner masses, such as those favored by the cosmological mechanism, remain beyond current limits and constitute targets for future higher-luminosity or higher-energy collider searches.

Overall, our results demonstrate that a heavier colored partner can serve as a temporary reservoir for a primordial baryon asymmetry and subsequently transfer this asymmetry to a self-conjugate dark matter particle. The mechanism operates through the interplay of QCD depletion, delayed portal conversion, and residual dark matter annihilation, and it can reproduce the observed relic abundance without requiring the dark matter particle itself to carry a conserved asymmetry or requiring a compressed spectrum. This framework thereby establishes a qualitatively distinct pathway from conventional asymmetric dark matter, in which a primordial baryon asymmetry can manifest as the observed dark matter density even when the dark matter particle is its own antiparticle. The simultaneous possibility of late cosmological conversion and detector-scale long-lived colored particles provides a direct connection between the relic-density mechanism and long-lived-particle searches at colliders.

CPC Accepted

Acknowledgments

F.L. and M.T. would like to thank S. Matsumoto, S. Shirai, and T.T. Yanagida for valuable discussions during their time at the Kavli IPMU. F.L. is supported by the Sun Yat-sen University Science Foundation.

References

[1] Planck collaboration, Astron. Astrophys. **641**, A6 (2020), arXiv: [1807.06209]
[2] D. Hooper, J. March-Russell and S.M. West, Phys. Lett. B **605**, 228 (2005), arXiv: [hep-ph/0410114]
[3] K.M. Zurek, Phys. Rept. **537**, 91 (2014), arXiv: [1308.0338]
[4] J. Kumar, AIP Conf. Proc. **1604**, 389 (2015), arXiv: [1308.4513]
[5] K. Petraki and R.R. Volkas, Int. J. Mod. Phys. A **28**, 1330028 (2013), arXiv: [1305.4939]
[6] D.E. Kaplan, M.A. Luty and K.M. Zurek, Phys. Rev. D **79**, 115016 (2009), arXiv: [0901.4117]
[7] J. Shelton and K.M. Zurek, Phys. Rev. D **82**, 123512 (2010), arXiv: [1008.1997]
[8] D. Suematsu, Astropart. Phys. **24**, 511 (2006), arXiv: [hep-ph/0510251]
[9] T. Cohen and K.M. Zurek, Phys. Rev. Lett. **104**, 101301 (2010), arXiv: [0909.2035]
[10] T. Cohen, D.J. Phalen, A. Pierce and K.M. Zurek, Phys. Rev. D **82**, 056001 (2010), arXiv: [1005.1655]
[11] A. Belyaev, M.T. Frandsen, S. Sarkar and F. Sannino, Phys. Rev. D **83**, 015007 (2011), arXiv: [1007.4839]
[12] H. An, S.-L. Chen, R.N. Mohapatra and Y. Zhang, JHEP **03**, 124 (2010), arXiv: [0911.4463]
[13] E. Nardi, F. Sannino and A. Strumia, JCAP **01**, 043 (2009), arXiv: [0811.4153]
[14] J.J. Heckman and S.-J. Rey, JHEP **06**, 120 (2011), arXiv: [1102.5346]
[15] H. Davoudiasl, D.E. Morrissey, K. Sigurdson and S. Tulin, Phys. Rev. Lett. **105**, 211304 (2010), arXiv: [1008.2399]
[16] N. Haba and S. Matsumoto, Prog. Theor. Phys. **125**, 1311 (2011), arXiv: [1008.2487]
[17] M. Blennow, B. Dasgupta, E. Fernandez-Martinez and N. Rius, JHEP **03**, 014 (2011), arXiv: [1009.3159]
[18] M.R. Buckley and L. Randall, JHEP **09**, 009 (2011), arXiv: [1009.0270]
[19] M.T. Frandsen, S. Sarkar and K. Schmidt-Hoberg, Phys. Rev. D **84**, 051703 (2011), arXiv: [1103.4350]
[20] L.J. Hall, J. March-Russell and S.M. West, *A Unified*

Theory of Matter Genesis: Asymmetric Freeze-In, 1010.0245.
[21] B. Dutta and J. Kumar, Phys. Lett. B **699**, 364 (2011), arXiv: [1012.1341]
[22] M. Dutta and N. Narendra, EPJ Web Conf. **312**, 05003 (2024)
[23] A. Falkowski, J.T. Ruderman and T. Volansky, JHEP **05**, 106 (2011), arXiv: [1101.4936]
[24] D. Borah, S. Mahapatra, P.K. Paul, N. Sahu and P. Shukla, Phys. Rev. D **110**, 035033 (2024), arXiv: [2404.14912]
[25] H. Iminniyaz, M. Drees and X. Chen, JCAP **07**, 003 (2011), arXiv: [1104.5548]
[26] M.L. Graesser, I.M. Shoemaker and L. Vecchi, JHEP **10**, 110 (2011), arXiv: [1103.2771]
[27] R. Rashidin, F. Liu and H. Iminniyaz, Nucl. Phys. B **1029**, 117570 (2026), arXiv: [2501.18209]
[28] K. Griest and D. Seckel, Phys. Rev. D **43**, 3191 (1991)
[29] M. Garny, J. Heisig, B. Lülf and S. Vogl, Phys. Rev. D **96**, 103521 (2017), arXiv: [1705.09292]
[30] J. Heisig, A. Lessa and L.M.D. Ramos, Phys. Rev. D **110**, 015031 (2024), arXiv: [2404.16086]
[31] C. Arina, *et al*, Eur. Phys. J. C **85**, 975 (2025), arXiv: [2504.10597]
[32] ATLAS collaboration, Phys. Rev. D **99**, 092007 (2019), arXiv: [1902.01636]
[33] ATLAS collaboration, JHEP **2306**, 158 (2023), arXiv: [2205.06013]
[34] A. De Simone, G.F. Giudice and A. Strumia, JHEP **06**, 081 (2014)
[35] K. Harigaya, K. Kaneta and S. Matsumoto, Phys. Rev. D **89**, 115021 (2014), arXiv: [1403.0715]
[36] J. Ellis, F. Luo and K.A. Olive, JHEP **09**, 127 (2015), arXiv: [1503.07142]
[37] H. An, M.B. Wise and Y. Zhang, Phys. Rev. D **93**, 115020 (2016), arXiv: [1604.01776]
[38] S.P. Liew and F. Luo, JHEP **02**, 091 (2017), arXiv: [1611.08133]
[39] J. Harz and K. Petraki, JHEP **07**, 096 (2018)
[40] H. Fukuda, F. Luo and S. Shirai, JHEP **04**, 107 (2019), arXiv: [1812.02066]
[41] W.-Y. Keung, I. Low and Y. Zhang, Phys. Rev. D **96**, 015008 (2017), arXiv: [1703.02977]
[42] M. Becker, E. Copello, J. Harz and M. Napetschnig, *Sommerfeld Effect and Bound State Formation for Dark Matter Models with Colored Mediators with SE+BSF4DM*, 2601.03026.
[43] J. Ellis, F. Luo, K.A. Olive and P. Sandick, Eur. Phys. J. C **73**, 2403 (2013), arXiv: [1212.4476]
[44] J. Ellis, J.L. Evans, F. Luo, N. Nagata, K.A. Olive and P. Sandick, Eur. Phys. J. C **76**, 8 (2016), arXiv: [1509.08838]
[45] R. Mertig, M. Bohm and A. Denner, Comput. Phys. Commun. **64**, 345 (1991)
[46] J. Edsjo and P. Gondolo, Phys. Rev. D **56**, 1879 (1997), arXiv: [hep-ph/9704361]
[47] K. Saikawa and S. Shirai, JCAP **05**, 035 (2018), arXiv: [1803.01038]
[48] E.W. Kolb and M.S. Turner, *The Early Universe*, vol. 69, Taylor and Francis (5, 2019), 10.1201/9780429492860.
[49] P. Gondolo and G. Gelmini, Nucl. Phys. B **360**, 145 (1991)
[50] D.J. Schwarz and M. Stuke, JCAP **11**, 025 (2009), arXiv: [0906.3434]
[51] M. D'Onofrio, K. Rummukainen and A. Tranberg, Phys. Rev. Lett. **113**, 141602 (2014), arXiv: [1404.3565]
[52] V. Simha and G. Steigman, JCAP **08**, 011 (2008), arXiv: [0806.0179]
[53] F. Di Clemente, A. Drago, L. Formaggio, C. Ratti, V. Vovchenko and G. Yadav, *Upper Bound on the Cosmic Baryon Chemical Potential from Lepton-Flavor Asymmetry*, 2511.11995.
[54] R.H. Cyburt, J. Ellis, B.D. Fields, F. Luo, K.A. Olive and V.C. Spanos, JCAP **10**, 021 (2009), arXiv: [0907.5003]
[55] M. Kawasaki, K. Kohri, T. Moroi, K. Murai and H. Murayama, JCAP **12**, 048 (2020), arXiv: [2006.14803]
[56] S. Bianco, J. Frerick, M. Hufnagel and K. Schmidt-Hoberg, *Improved Big Bang Nucleosynthesis constraints on decaying massive relics*, 2605.26824.
[57] ATLAS Collaboration, "Search for heavy, long-lived, charged particles with large ionisation energy loss in *pp* collisions at $\sqrt{s}$ = 13 TeV using the ATLAS experiment and the full Run 2 dataset (Version 1)." HEPData collection, doi:10.17182/hepdata.127994.v1, 2022.
[58] J. Alwall, R. Frederix, S. Frixione, V. Hirschi, F. Maltoni, O. Mattelaer, *et al*, JHEP **07**, 079 (2014), arXiv: [1405.0301]
[59] C. Bierlich, *et al*, SciPost Phys. Codeb. **2022**, 8 (2022), arXiv: [2203.11601]
[60] W. Beenakker, C. Borschensky, M. Krämer, A. Kulesza and E. Laenen, JHEP **12**, 133 (2016), arXiv: [1607.07741]
[61] CMS collaboration, Phys. Rev. D **104**, 012015 (2021), arXiv: [2012.01581]
[62] O. Cerri, S. Xie, C. Pena and M. Spiropulu, JHEP **04**, 037 (2019), arXiv: [1807.05453]
[63] ATLAS collaboration, JHEP **07**, 140 (2025), arXiv: [2502.06694]
[64] T. Cohen, R.T. D'Agnolo, M. Hance, H.K. Lou and J.G. Wacker, JHEP **11**, 021 (2014), arXiv: [1406.4512]

CPC Accepted